ANAS Transactions **Earth Sciences** **1 / 2024**

http://www.journalesgia.com

INTEGRATED 2D GEOELECTRIC PROSPECTING FOR GOLD MINERALIZATION POTENTIAL WITHIN SOUTHERN PART OF KEBBI NW NIGERIA

Augie A.I.[1,2], Salako K.A.[2], Rafiu A.A.[2], Jimoh M.O.[3]

[1]Department of Applied Geophysics, Federal University Birnin Kebbi, Nigeria: ai.augie@fubk.edu.ng

[2]Department of Geophysics, Federal University of Technology Minna, Nigeria

[3]Department of Geology, Federal University of Technology Minna, Nigeria

Keywords: *2D Modelling, Electrical Resistivity Tomography, Induced Polarization, Self-Potential, gold mineralization*

Summary. This is a detailed geophysical research into the anomalous zones identified by previous aeromagnetic studies in the area. Integrated 2D geoelectric prospecting methods involving ERT, IP and SP techniques were used to delineate subsurface structure suitable for gold mineralization potential in parts of the Yauri, Shanga, and Magama areas of the states of Kebbi and Niger in the northwest Nigeria. The ERT, IP and SP measurements were carried out with a dipole-dipole configuration and the SuperSting resistivity meter. The research results revealed regions with low/high resistivity, high chargeability, and high SP values, which were identified as mineral potential zones. The ERT technique has helped to delineate regions with low resistivity anomalous which correspond to oxidized rocks associated with granite/quartzite veins. High resistivity range could exist over dyke structures associated with partially decomposed granite and quartzite, as indicated by the geological setting and borehole log of the area. The IP technique revealed a high chargeability (≥ 20 milliseconds) in the study area, possibly due to the accumulation of metallic minerals in host rocks, such as gold. The SP technique has also helped to identify regions with high SP anomalies (≥20 mV), which are characterized by vein-bearing ore minerals. The integration of ERT, IP, and SP results revealed oxidized rock zones, dyke subsurface structures of decomposed quartzite, granite, gneiss, and ore mineral veins. These zones are located in the northwest Mararraba, the southwest Jinsani, and the southern Sabon Gari in Niger and Kebbi states. The areas could be considered a potential pathway for gold exploration and exploitation.

1. Introduction

There are many areas of gold occurrence in Nigeria mainly associated with the schist belts which are composed of rocks like gneisses, schists, quartzites, amphibolites and granitoids (Olalekan et al., 2016; Ejepu et al., 2018). Gold mines are very important economic assets for many countries in the world including Nigeria in particular, therefore these activities require a geophysical approach that will delineate possible pathways for gold exploration and exploitation (Augie and Ridwan, 2021; Augie et al., 2021a). Two-dimensional electrical resistivity tomography (ERT), induced polarization (IP) and self-potential (SP) are some of the geophysical methods used for mapping the potential zones, especially those of gold (Bagare et al., 2018). Oduduru and Mamah (2014) revealed that the integration of electrical resistivity tomography and IP methods can be powerful and effective diagnostic tools to delineate geologic structures and for the identification of strata. The IP technique has been used over the past 30 years with proven potential in providing in-situ information about rock mineralogy, particularly in the search for disseminated minerals with electronic conductivity (Unuevho et al., 2016; Amoah et al., 2018).

Various field mapping exercises were conducted in the southern part of Kebbi NW Nigeria with the view of assessing the mineralization potential using aeromagnetic data alone. Consequently, mineralization potentials have been reported in the area by these studies (e.g. Ramadan and Abdel-Fattah, 2010; Bonde et al., 2019; Lawali et al., 2020; Lawal et al., 2021; Augie et al., 2021a, 2022b and 2022c). Results from these studies reveal major structural trends in the area oriented along ENE-WSW, NE-SW and E-W directions while minor trends were along NW-SE, NNE-SSW, NNW-SSE and N-S directions of the area. These results are generally concordant with the main regional structural trend dipping to the NW. The results also revealed that the southern part of the Kebbi,

NW Nigeria is dominantly a basement complex, which may play host to economic minerals. Augie et al. (2021b, 2022b, 2022c) further revealed that the structures delineated within the area when compared with the geological setting, correspond to quartz-mica schist, granite, biotite, gneiss, diorite, medium coarse-grained and biotite hornblende granite. The regions correspond to SE parts of Yauri and Shanga, Fakai, Ngaski, Zuru, Magama, Rijau, and the eastern part of Wasagu/Danko and Bukkuyum.

However, previous studies have only used aeromagnetic data and the anomalous zones detected from the aeromagnetic studies were not followed up by detailed work. A combined 2D ERT, IP and SP geophysical methods for gold prospects and their associated mineralization have not been conducted in the area. The 2D ERT would be used to unveil lithological boundaries and geologic structures such as faults, dykes, veins and other mineral trapping structures associated with gold-bearing alteration zones (Loke and Barker, 1996; Loke, 2004). Likewise, IP and SP methods are particularly useful for detecting disseminated minerals that are difficult to detect using resistivity alone (Unuevho et al., 2016). This integrated method would be employed to delineate gold mineral-bearing zones and lithological boundaries. The IP, SP and Resistivity are some of the geophysical methods used for mapping the gold minerals as they contribute to better-fined targets. The inversion of resistivity, IP and SP data could throw light into the subsurface by tomographic and other pattern analyses associated with gold mineralization (Shao et al., 2021).

This paper used data from 2D electrical resistivity tomography, induced polarization and self-potential data with the view to delineate the gold-bearing alteration zones and other subsurface striations as a potential host for other mineralization. The results from these techniques were used to map probable gold anomalous zones within the study area where detailed exploration for the gold can be concentrated. The dipole-dipole array was adopted because of its low EM (electromagnetic) coupling between the current and potential circuits, very sensitive to horizontal and vertical changes in resistivity. It is good for mapping vertical structures, such as dykes and cavities. It has a better resolution than both Wenner and Schlumberger configurations (Loke and Barker, 1996; Loke, 2004).

2. Theoretical Framework and Field Procedures

In geoelectrical methods, the current is driven through one pair of current-electrodes (A and B) and the potential differences are measured with the aid of pair of potential-electrodes (M and N) connected to a sensitive voltmeter called a Resistivity meter (Telford et al., 1990; Augie et al., 2022a). This will possibly determine an effective or apparent resistivity of the subsurface as shown in Fig. 1:

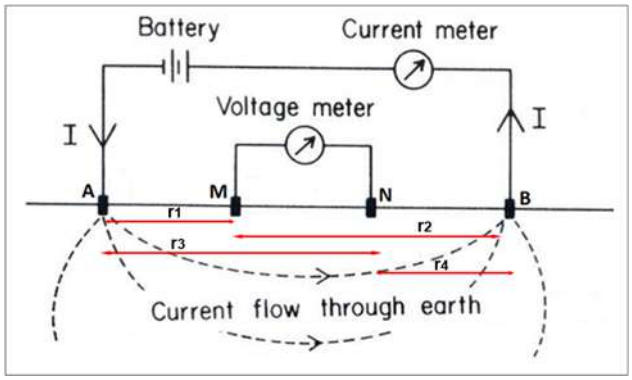

Fig. 1. Diagram used to determine the potential difference between two points

Ohm's law described that resistance (R) which is usually measured in ohm of a rock or particular sample is directly proportional to the length (L) of the resistive material (i.e., earth materials) and inversely proportional to its cross-sectional area (A) as given in equation (1):

$$\mathrm{R}\,\alpha\,\frac{L}{A} \tag{1}$$

$$\mathrm{R} = \rho\frac{L}{A} \tag{2}$$

where

ρ, the constant of proportionality called electrical resistivity. Electrical Resistivity is independent of the shape or size of the material but there are factors which affect the electrical resistivity such as moisture content, composition of strata, temperature and electrolytes. It is the true resistivity, and the resistivity values of rocks and minerals can be classified as good conductors, bad conductors, or isolators (Dahlin and Zhou, 2004).

According to Ohm's law:

$$\mathrm{R} = \frac{\Delta V}{I} \tag{3}$$

and

$$\Delta V = V_2 - V_1 \tag{4}$$

where; ΔV is the potential difference between the earth materials, I is the electric current through it and R is the resistance of the earth materials.

Substituting equation (3) into (2):

$$\frac{\Delta V}{I} = \rho\frac{L}{A} \tag{5}$$

This implies:

$$\rho = \frac{\Delta V}{I}\left(\frac{A}{L}\right) \tag{6}$$

where
$A = 2\pi r^2$ (hemispherical area under the earth) and $r = L$ (distance away from the source).

The potential difference (ΔV):

$$\Delta V = \frac{I\rho}{2\pi r} \tag{7}$$

$$\Delta V = \frac{I\rho}{2\pi}\left(\frac{1}{r}\right) \tag{8}$$

r is the distance between the current electrode point and the point where potential is measured.

Total potential at M due to current electrodes A and B (see Fig. 1);

$$V_{M\,(A,B)} = \frac{I\rho}{2\pi}\left(\frac{1}{r1} - \frac{1}{r2}\right) \tag{9}$$

Total potential at N due to current electrodes A and B;

$$V_{N\,(A,B)} = \frac{I\rho}{2\pi}\left(\frac{1}{r3} - \frac{1}{r4}\right) \tag{10}$$

The net potential difference is:

$$\Delta V_{MN\,(A,B)} = V_{M\,(A,B)} - V_{N\,(A,B)} \tag{11}$$

$$\Delta V_{MN\,(A,B)} = \frac{I\rho}{2\pi}\left(\frac{1}{r1} - \frac{1}{r2} - \frac{1}{r3} + \frac{1}{r4}\right) \tag{12}$$

$$\rho = \frac{\Delta V}{I} 2\pi \left(\frac{1}{\frac{1}{r1} - \frac{1}{r2} - \frac{1}{r3} + \frac{1}{r4}}\right) \tag{13}$$

and

$$K = 2\pi \left(\frac{1}{\frac{1}{r1} - \frac{1}{r2} - \frac{1}{r3} + \frac{1}{r4}}\right),\ R = \frac{\Delta V}{I} \tag{14}$$

Therefore

$$\rho = \mathrm{KR} \tag{15}$$

where; K is the geometrical factor of the electrode arrangement.

Time-domain IP estimations include observing the decaying voltage after the current is turned off. The most ordinarily measured parameter is the chargeability M, defined as the area A beneath the decay curve over a certain time interval standardized by the consistent state potential difference ΔVc (Bagare et al., 2018).

$$\mathrm{M} = \frac{\mathrm{A}}{\Delta \mathrm{V_c}} = \frac{1}{\Delta \mathrm{V_c}} \int_{t_1}^{t_2} \mathrm{v(t)\,dt} \tag{16}$$

Chargeability is measured over a specific time stretch not long after the polarizing current is cut off. Area A is determined within the measuring apparatus by analogue integration. Different minerals are distinguished by characteristic chargeabilities, for example, pyrite has M = 13.4 ms over an interval of 1 s, and magnetite 2.2 ms over the same interval (Bagare et al., 2018).

The total SP anomaly can be defined as (Fedi and Abbas, 2013)

$$S(P) = \int_V^0 \nabla \cdot \frac{\boldsymbol{K}}{r}\, dr \tag{17}$$

where, K is the electric dipole moment due to charge accumulation, either primary or induced, and r is the distance from the observation point P.

The streaming potential E_k which η is observed when a solution of electrical resistivity ρ and viscosity ρ is forced through the capillary of the porous medium. The resultant potential difference between the ends of the passage is: (Telford et al., 1990; Jamaluddeen et al., 2014; Augie et al., 2022a)

$$E_k = -\frac{\xi \Delta P K_p}{4\pi\eta} \tag{18}$$

where ξ is the adsorption potential, ΔP is the pressure difference and Kp is the solution dielectric constant.

2.1 Location and Geological Setting of the Study Area

The fieldwork was conducted in some selected areas of the Kebbi and Niger States. These areas are Shanga (Sabon Gari) and Yauri/Ngaski boundaries (Mararraba) of Kebbi state, and also Magama (Irana) of Niger State NW Nigeria (see Fig. 3). The study areas lie between latitudes 11°5′10″N to 11°5′40″N and longitudes 4°43′0″E to 4°43′25″E (Sabon Gari), latitudes 10°47′55″N to 10°48′20″N and longitudes 4°42′0″E to 4°54′0″E (Mararraba), and latitudes 10°31′40″N to 10°32′20″N and longitudes 4°55′59″E to 4°56′15″E (Irana).

Geologically, the study area falls under the basement complex rocks associated with: granite, rhyolite, biotite-granite, meta-conglomerate, quartz-mica schist, migmatite, undifferentiated schist including gneiss, biotite gneiss, medium coarse-grained and biotite-hornblende granite (Fig. 2). The southern part of Kebbi of the basement complex/schist belt is called Zuru-Yauri Schist Belts (Danjumma et al., 2019; Olugbenga and Augie, 2020), consist of an assemblage of muscovite-biotite banded gneisses, porphyroblastic gneisses, migmatites, schists, quartzites, metavolcanics (amphibolites), quartzites, mica schists, granulites, calc-silicates older granites and minor rocks such as gabbro, andesite, granulites and calc-silicates.

The structural elements in Zuru Schist Belt are the major NNE-SSW to NE-SW trending B/Yauri, Yauri and Ribah dextral faults, an NW-SE trending Gunu sinistral fault and a major N-S trending anticlinorium called the Zuru anticlinorium (Sani et al., 2019; Danbatta, 2005). These schists are lithologically different from the other schists belt in northwestern Nigeria and it is predominantly composed of quartzites with very subordinate schists and amphibolites (Danjumma et al., 2019; Danbatta, 2008).

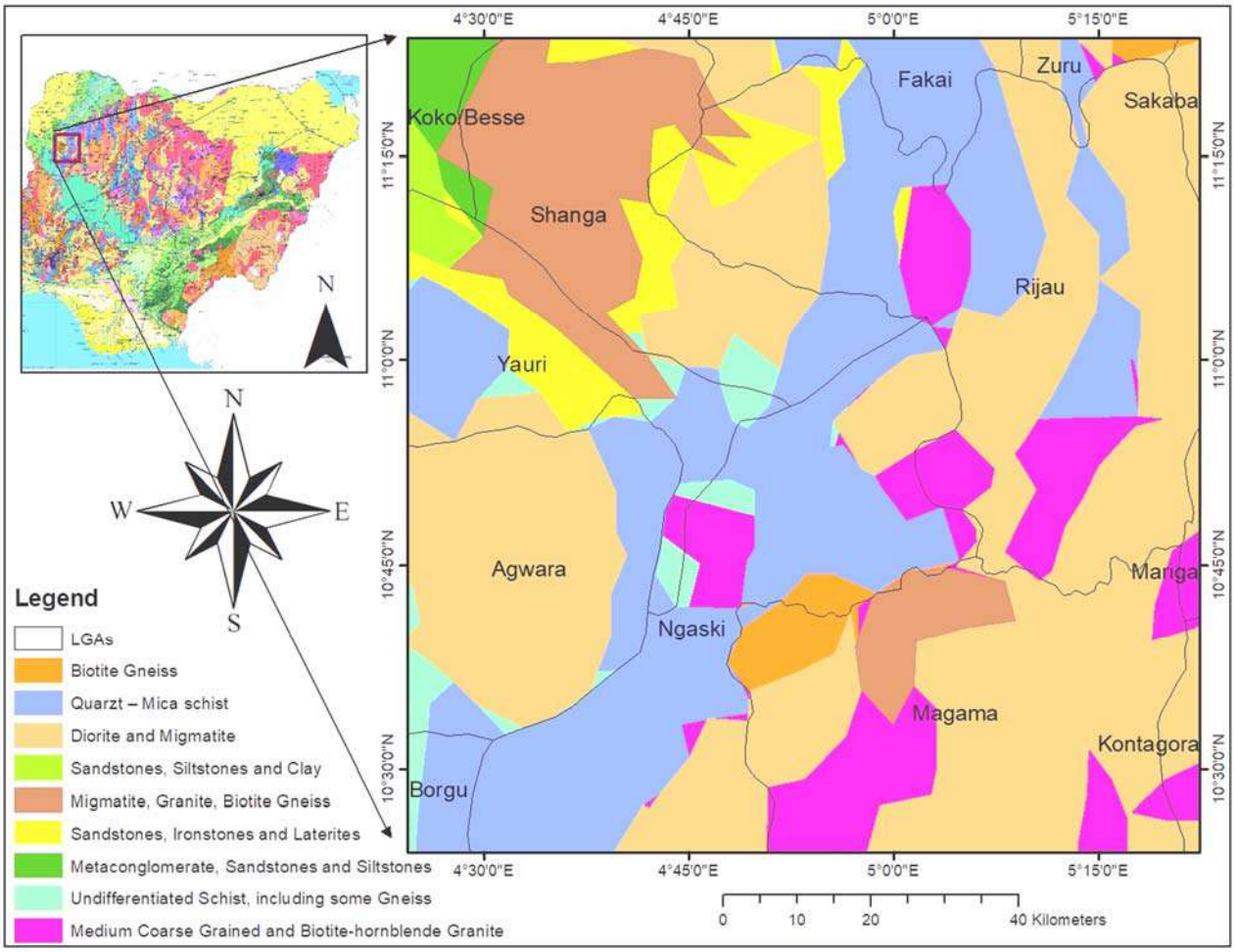

Fig. 2. Location and geological map of the study area

3. Methodology

In this study, a 2D geoelectrical survey was carried out at Yauri/Ngaski boundaries (Mararraba), Shanga (Sabon Gari) of Kebbi state, and also Magama (Irana) of Niger State NW Nigeria. An area of 490 m^2, 640 m^2, and 490 m^2 fields were investigated using a dipole-dipole configuration with minimum electrode spacing (a) of 10.00 m. A total of 7 profiles were designed for each 300 m distance along the profile, oriented NW-SE (Fig. 3). Profiles 1 and 2 were conducted at Magama (Irana), profiles 3 and 4 – at Shanga (Sabon Gari), and profiles 5, 6, and 7 – at Yauri/Ngaski boundaries (Jinsani and Mararraba).

The data was taken with the aid of Super Sting (resistivity meter) coupled with an electrode selector and powered by a 12 V battery. This instrument has the capability of measuring apparent resistivity, IP, and SP data. It has a transmitter with automatic/or user selectable currents in milliamps as; 1, 2, 5, 10, 20, 50, 100, 200, 500 and 1000 mA. The distance, between the two current electrodes (C1 and C2), is the same as that between the potential electrodes (P1 and P2). Distance between the current electrode C1 and the potential electrode P1 (dipole separation factor) was made in multiple of an integer n of the distance between the current and potential electrode pair (Fig. 4).

Initially, the dipole separation factor n was set to be 1, then it is increased to 2, 3, and so on until a maximum value of 8. Thus, both the dipole separation factor (n) and the spacing between the current electrode pair (a) were recorded. Measurements were done at an electrode spacing of 10 m and n was set at 1, 2, 3, up to 8 (Fig. 4). The more the increase in n which would equally increase the electrode spacing, the more the injected current flows to greater depths (Loke and Barker, 1996).

For the first measurement, electrodes number 1, 2, 3, and 4 were used. Electrode 1 was used as the second current electrode (C2) at 0 m, electrode 2 as the first current electrode (C1) at 10 m, electrode 3 as the first potential electrode (P1) at 20 m, and electrode 4 as the second potential electrode (C2) at 30 m.

Likewise, in the second measurement, electrodes number 1, 2, 3, and 4 were used for C2 at 10 m, C1 at 20 m, P1 at 30 m, and P2 at 40 m respectively. These procedures were repeated down the profile line using 1a 2a, 3a, 4a, 5a, 6a, 7a, and 8a spacing between C1 and P1 where a is 10 m.

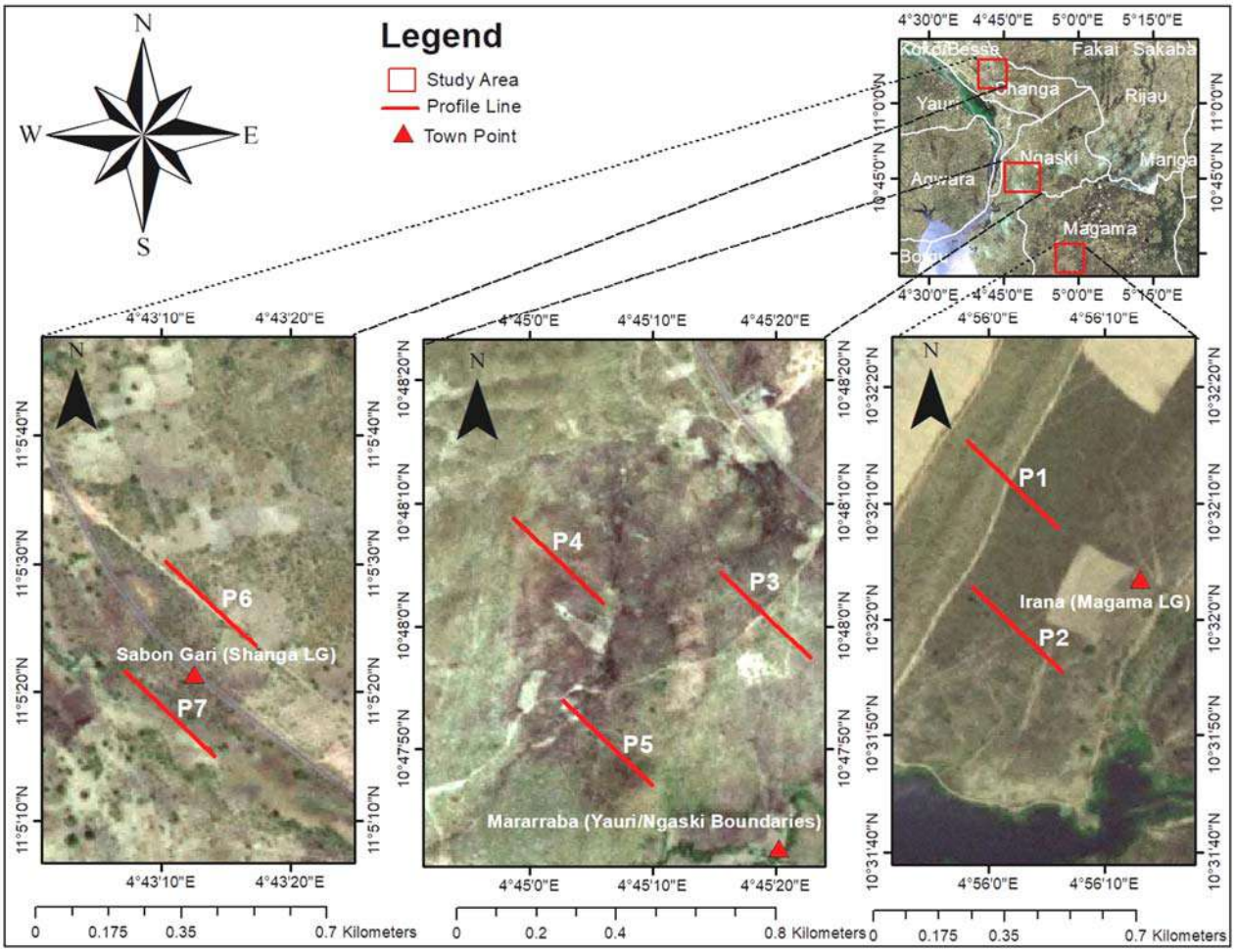

Fig. 3. Field survey layout using the dipole-dipole electrode configuration

At each measurement, the measured ground apparent resistivity, IP, and SP data were obtained. The acquired data were processed with the RES2DINV program developed by Loke (2004), which automatically determines a 2D resistivity and IP models for the subsurface. SP data were also analyzed and processed using surfer software version 13.

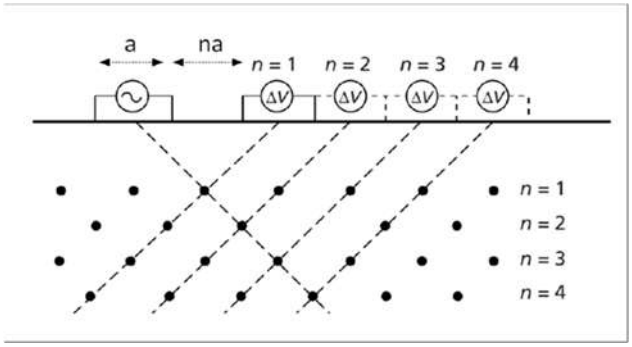

Fig. 4. Illustration of dipole-dipole array and pseudosection for putting the measured apparent resistivity and IP (Wahyu et al., 2016)

4. Result

In this study, the interpretation of the 2D geoelectric modeled sections is associated with the geological setting of the area. These include the borehole lithology of the southern part of Kebbi obtained from RUWASA (Rural Water Supply and Sanitation Agency) as shown in Table 1 and resistivity values obtained from previous works in the same basement complex which were used to correlate the results of the present survey (Osazuwa and Chii, 2010).

The sections have a vertical axis (y-axis) corresponding to the depth of investigation and a horizontal distance axis (x-axis) representing distance along the profile. The inverse section of each profile was interpreted in terms of geology (Fig. 2) and related information. The summary of results obtained from the integrated methods is given in Table 2.

Table 1

A borehole/lithology log of southern part of Kebbi areas (SARDA, 1988; Osazuwa and Chii, 2010)

Lithology	Depth(m)	Thickness(m)	Resistivity range (Ωm)
Lateritic Sand	0-2	2	60-1000
Highly Decomposed Schist	2-10	8	10-500
Partially Decomposed Granite	10-15	12	100-1000
Quartzite's and Gneiss	15-21	16	200-100000

4.1 Resistivity Model Section for Profile 1 (P1)

Profile 1 covers a lateral extent of 300 m (Fig. 5a). It is oriented in the NW-SE direction and lies between latitudes 10°32′13.2″N to 10°32′6″N and longitudes 4°56′6″E to 4°55′58″E (Fig. 3). The subsurface features from Fig. 5(a) could be sectionalized into four: **A**, **B**, **C**, and **D** zones. Zone **A** is characterized by low resistivity values ranging from 117 Ωm to 944 Ωm. It has a lateral length of 5-45 m, 55-102 m, 145-165 m, and 241-285 m at a depth/thickness of 19 m, 19-24.9 m, 19 m, and 17-24.9 m. Zone **B** has resistivity values of 945 Ωm to 7638 Ωm. This zone occupied a length of 50-90 m and 60-105 m, at a depth/thickness of 13 m and 18.5-20 m respectively. **C** is characterized by resistivity values ranging from 7639 Ωm to 21728 Ωm and it occupied the distance along the profile from 90-165 m at a depth/thickness of 18.5 m. However, zone **D** is characterized by the resistivity of 61815 Ωm to 175857 Ωm, it has a length of 90-140 m and 160-250 m with a corresponding depth/thickness of 7.5-24.9 m and 24.9 m.

The suggested subsurface lithology for features **A**, **B**, **C**, and **D** from Table 1, could be lateritic soil, highly decomposed schist, partially decomposed granite and quartzite, and quartzite/gneiss. However, low resistivity regions of **A** could be a result of water content and weathering in the oxidized rock. Some minerals, particularly gold, could be hosted mostly in a rock corroded by water called oxidized rocks, mainly of granite or rhyolite origin. Zone **C** of partially decomposed granite and quartzite has formed the dyke structures. Dyke subsurface structures of decomposed granite and quartzite usually play a pivotal role in determining the gold mineral. Zone **D** is the region with the highest resistivity. When compared to the borehole log and geological setting of the area, the region is underlain by quartzite and gneiss. These highest resistivity regions could be caused by the inclusion of impurity ions into particular minerals, which has a significant effect on resistivity of the zone. The results of the inverse model section (Fig. 5a) were indicated in the geologic section as given in Fig. 5(b).

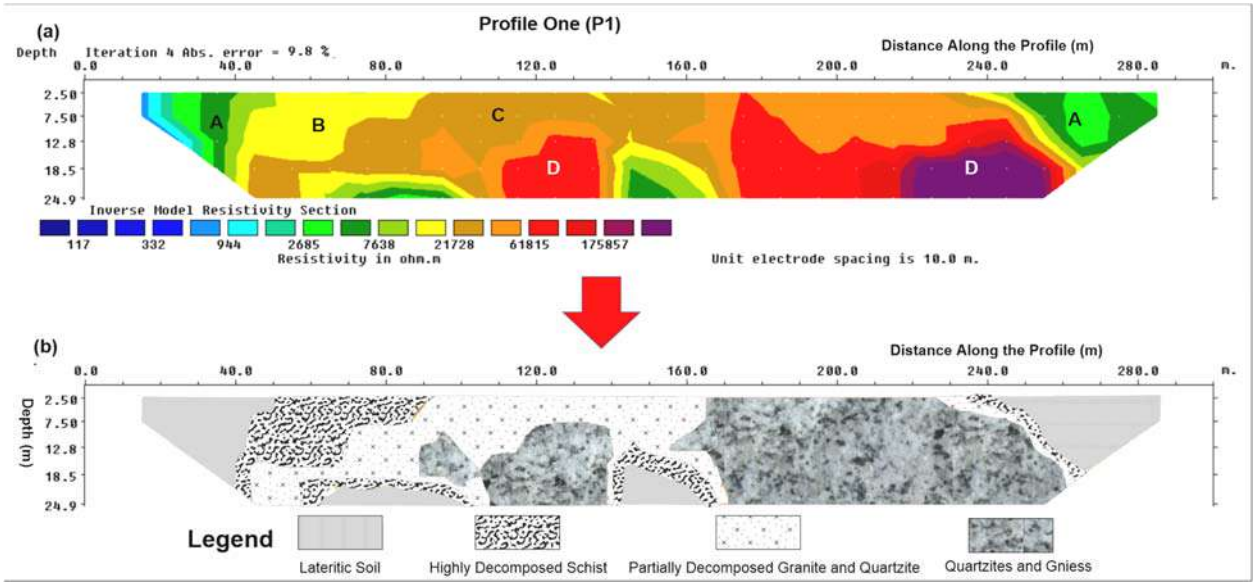

Fig. 5. (a) Inverse Model Resistivity Section and (b) Geologic Section for the Dataset Along Profile One (P1)

4.2 IP Model Section for Profile 1 (IP1)

Fig. 6 shows the inverse model chargeability section of profile one (IP1) which revealed the signatures of minerals. The model shows zones (**A1**) with the highest chargeability values ranging from 38.4 to 290 msec along the profile. It occupied the x-position of 120-140 m and 170-190 m and appeared at a depth/thickness of 18.5-24 m and 12.8 m. These regions with higher chargeability were further extended to 230-260 m and 205-290 m along the profile at a depth of 18.5 m and 24.9 m respectively. Higher chargeability usually occurs as a result of an accumulation of metallic minerals in host rocks such as gold minerals. These regions could be considered as a potential target for exploration particularly metallic minerals, particularly gold mineralization.

4.3 SP Section for Profile 1 (S1)

Fig. 7 gives the results of the SP section along profile one (S1). The sections revealed the high SP values ranged from 20 mV and above. They occupied the x-positions of 0-10 m, 55-75 m, and 120-140 m at a depth/thickness of 50 m, 80 m, and 40 m. These regions were labeled as zone **A2**. High SP values could occur as a result of either the reduction-oxidation effect associated with ore bodies and organic matter-rich-contaminants, or the streaming potential which is related to water flow (Lobo-Guerrero, 2004). For this, the regions with high SP values were characterized by vein (i.e quartz vein as compared with Fig. 2) bearing ore minerals. The veins could be associated with gold mineralization as compared with the geological setting coupled with the borehole log of the area (Table 1).

4.4 Resistivity Model Section for Profile 2 (P2)

The 2D inverse section for P2 situated in the NW-SE direction was given in Fig. 8(a). It covers a length of 300 m and lies between latitudes 10°32′2.4″N to 10°31′55.2″N and longitudes 4°55′56.6″E to 4°58′8″E (see Fig. 3). The subsurface section in Fig. 8(a) was categorized into four zones: **A**, **B**, **C**, and **D**. Zone **A** is described by low resistivity values ranging from 113 Ωm to 594 Ωm, it has a sidelong length of 10-30 m, 160-165 m, and 202-222 m at a depth/thickness of 12 m, 24.9, and 2.5 m respectively. Zone **B** has resistivity values of 1359 Ωm to 3112 Ωm, it has occupied a lateral distance of 12-41 m, 50-80 m, 110-160 m, 169-230 m, 231-249 m, and 270-285 m, and a corresponding depth/thickness of 24.9 m, 24.9 m, 12.8, 18.5 m, 24.9 m, and 18.5 m, respectively. **C** is portrayed by resistivity values going from 3113 Ωm to 7123 Ωm, it covers the distance along the profile from 41-50 m and 81-120 m and a depth/thickness of each 18.5 m. Nonetheless, zone **D** is portrayed by the resistivity of 7124 Ωm to 37331 Ωm, it has occupied a length of 41-70 m, 50-80 m, 110-160 m, 169-230 m, 170-220 m, 231-249 m, and 270-285 m at a corresponding depth/thickness of 12-24.9 m, 7.5-12 m, 12-24.9 m, 13.0-24.9 m and 250-270 m respectively.

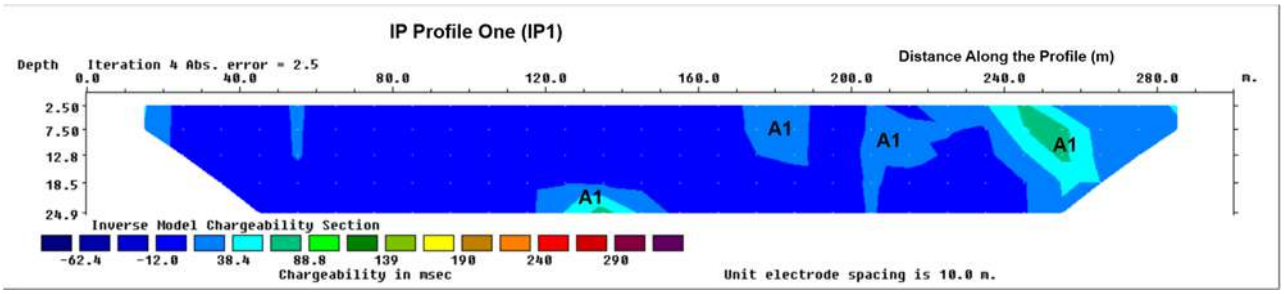

Fig. 6. Inverse Model Chargeability Section for Profile One (IP1)

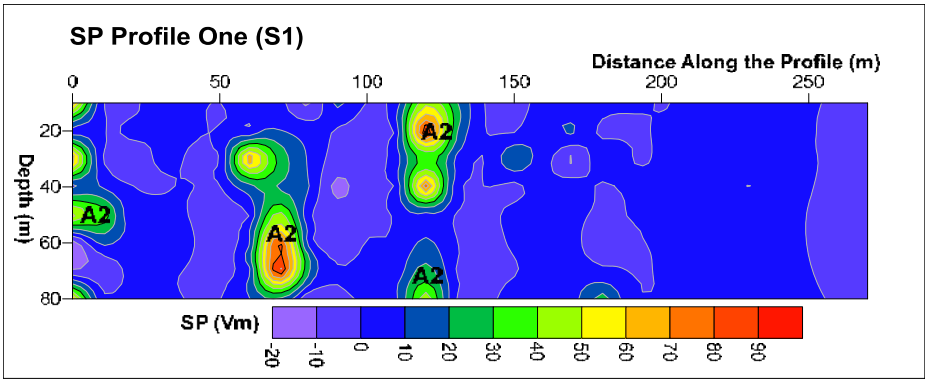

Fig.7. SP 2D Section for Profile One (S1)

The subsurface lithology for highlights **A**, **B**, **C**, and **D** from Table 1 could be lateritic soil, highly decomposed schist, partially decomposed granite and quartzite, and quartzite/gneiss. However, the low resistivity signature (zone **A**) in these regions could be a result of water content and weathering in the oxidized rock. This type of rock is mainly of granite or rhyolite origin. It could host some metallic minerals, particularly gold. Zone **C** has formed the dyke subsurface structures of decomposed granite and quartzite. These structures could play a pivotal role in determining the gold minerals. The results of the inverse model section given in Fig. 8(a), were transformed into a geologic section as shown in Fig. 8(b).

4.5 IP Model Section for Profile 2 (IP2)

The 2D inverse model chargeability section for profile two (IP2) was given in Fig. 9. The section has revealed the signature of minerals namely zones **A1**. These zones have the highest chargeability values ranging from 35 msec and above, which are located on along the x-positions of 35-60 m, 50-85 m, 140-175 m, 110-195 m, 198-220 m and 230-250 m at a depth/thickness of 12.8-24.9 m, 12.8 m, 12.8-24.9 m 12.8 m, 7.5 m and 18.5 m respectively. Higher chargeability of zones **A1** could occur as a result of an accumulation of metallic minerals in host rocks. These regions with high chargeability could be considered as a potential target for the exploration of metallic minerals such as gold mineralization.

4.6 SP Section for Profile 2 (S2)

The results of the SP section along with profile one (S1) were given in Fig. 10. The sections under the x-position of 0-54 m, 50-60 m, 61-100 m, 145-155 m, 160-210 m and 115-140 m at corresponding depth/thicknesses of 80 m, 80 m, 20-65 m, 40 m, 60 m, and 80 m have high SP values ranging from 20 mV and above. These areas were named zone **A2.** High SP values could happen because of either reduction-oxidation impact related to mineral bodies and natural matter-rich-pollutants, or the streaming potential which is connected with fluid flow. The zones with high SP signatures were described by vein-bearing metallic minerals. These veins could be related to gold mineralization as compared with the geological setting combined with the borehole log of the area.

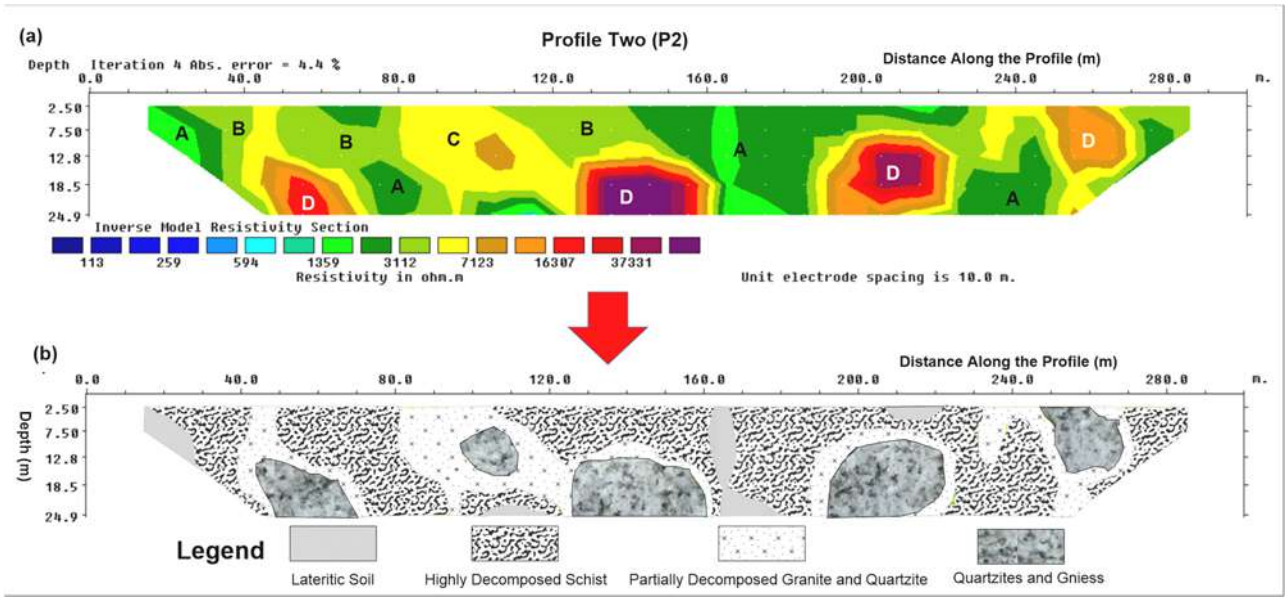

Fig. 8. (a) Inverse Model Resistivity Section and (b) Geologic Section for the Dataset along Profile Two (P2)

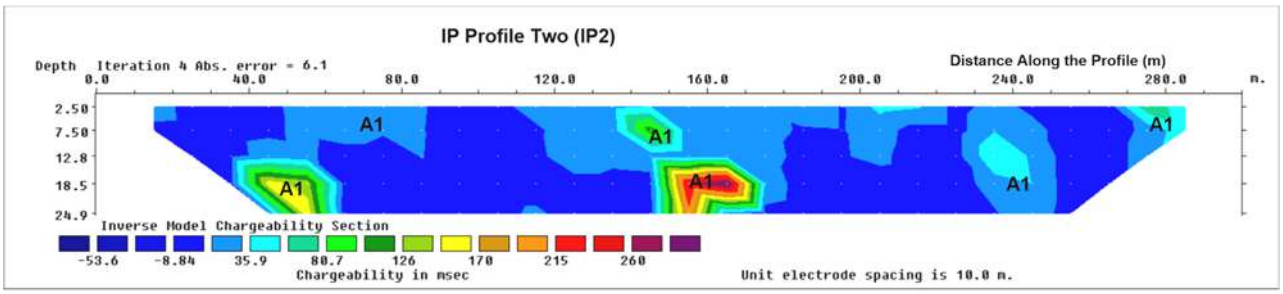

Fig. 9. Inverse Model Chargeability Section for Profile Two (IP2)

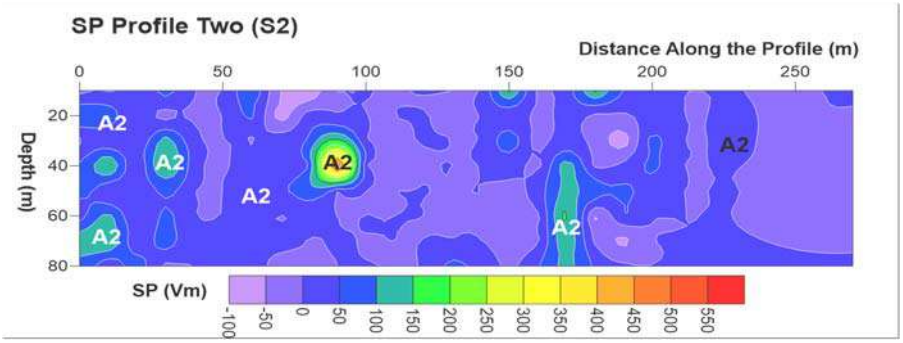

Fig. 10. SP 2D Section for Profile Two (S2)

4.2.7 Resistivity Model Section for Profile 3 (P3)

Fig. 11(a) is the 2D inverse model section for profile 3. It is oriented in the NW-SE direction and has a lateral distance of 300 m. The profile lies between latitudes 10°47′56.4″N to 10°48′3.6″N and longitudes 4°45′7.2″E to 4°45′18″E (see Fig. 3.). The subsurface feature was sectionalized into four different zones namely: **A**, **B**, **C**, and **D**. Zone **A** is characterized by resistivity values ranging from 1.6 Ωm to 459 Ωm, and are located on 10-80 m, 190-200 m, 250-265 m along the profile and a depth/thickness of 12.0 m, 18.5-24.9 m and 7.5-18.5 m respectively. **B** has resistivity values of 460 Ωm to 1888 Ωm, it covers a length of 30-110 m, 130-149 m, 190-200 m and 245-265 m at a corresponding depth/thickness of 2.5-18.5 m, 24.9 m, 18.5 m and 2.5-18.5 m. **C** is characterized by resistivity values going from 1889 Ωm to 7773 Ωm, it covers the distance along the profile of 35-55 m, 70-92 m, 105-130 m, 145-180 m, 200-210 m and 220-270 m and a depth/thickness of 8-24.9 m, 3-24.9 m, 24.9 m, 24.8 m, 24.9 m and 7.5 m. Likewise, zone **D** is portrayed by the resistivity of 7774 Ωm to 32002 Ωm, it has occupied a length of 100-125 m, 175-190 m, 200-250 m and 265-290 m at a corresponding depth/thickness of 7.5-24.9 m, 12-24.9 m, 2.5-24.9 m and 18.5 m respectively.

The subsurface lithology for features **A**, **B**, **C**, and **D** as compared with Table 1 could be lateritic soil, highly decomposed schist, partially decomposed granite and quartzite, and quartzite/gneiss. However, zone **A** of low resistivity areas could result from water content and enduring in the oxidized rock. Some minerals, especially gold, could be facilitated by this kind of oxidized rock that originates from granite or rhyolite. Zone **C** is associated with partially decomposed granite and quartzite which form dykes. Dyke subsurface structures of the aforementioned rock formation could play a pivotal role in determining the gold mineral. The results of the inverse model section given in Fig. 11(a) were further transformed into a geologic section as shown in Fig. 11(b).

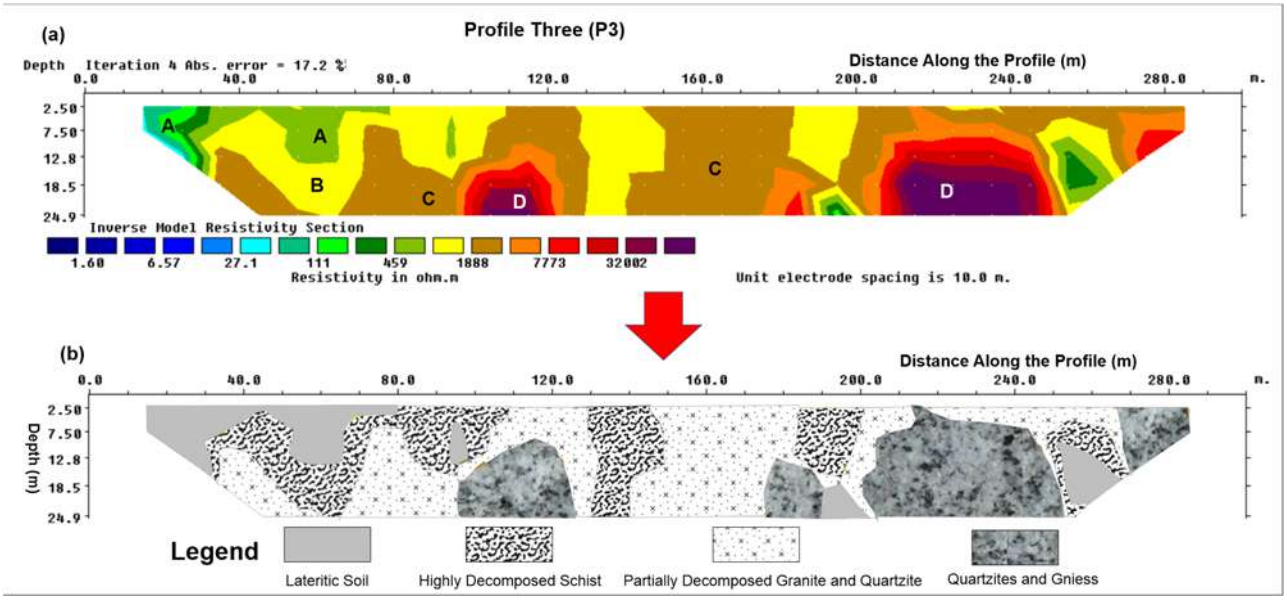

Fig. 11. (a) Inverse Model Resistivity Section and (b) Geologic Section for the Dataset along Profile Three (P3)

4.8 IP Model Section for Profile 3 (IP3)

The results of 2D inverse model chargeability sections along profile three (IP3) were given in Fig. 12. The sections revealed clearly the regions where exhibit metallic minerals, namely zone **A1**. These regions have the most noteworthy chargeability values ≥ 20 msec. The zone covers an x-position of 45-60 m, 190-202 m and 202-255 m at a corresponding depth/thickness of 7.5-18.5 m, 7.5 m and 12.8-24.9 m. The higher chargeability of zone **A1** generally happens because of the collection of metallic minerals in host rocks. These locales could be considered as a possible objective for the investigation of specific metallic minerals, particularly gold mineralization.

4.9 SP Section for Profile 3 (S3)

The results of the 2D SP section along profile one (S1) were given in Fig. 13. The regions with high SP (≥ 40 mV) signatures were labeled as zone **A2**. It has a lateral distance of 0-40 m, 50-60 m, 70-100 m, 120-200 m, 140-135, 190-240 m and a depth/thickness of 70 m, 21 m, 21-41 m, 15 m, 80 m and 21-80 m respectively. These regions with high SP signatures were depicted by veins, bearing metallic minerals. And these veins could be connected with gold mineralization as compared with the geological setting coupled with the borehole log of the area.

4.10 Resistivity Model Section for Profile 4 (P4)

Profile 4 covers a lateral extent of 300 m (Fig. 14a). It is oriented in the NW-SE direction and lies between latitudes 10°48′0″N to 10°48′7.2″N and longitudes 4°44′52.8″E to 4°45′0″E (see Fig. 3). The subsurface variations of resistivity were categorized into zone **A**, **B**, **C** and **D**. **A** is characterized by resistivity values ranging from 4.6 Ωm to 601 Ωm, it covers a lateral distance of 5-40 m, 165-185 m, 245-260 m, and a depth/thickness of 7.5 m, 18.5-24.9 m and 18.5-24.9 m respectively. **B** has resistivity values of 602 Ωm to 2033 Ωm, it covers a length of 40-90 m, 120-150 m, and 155-190 m at a corresponding depth/thickness of 12 m, 7.5 m and 18.5-24.9 m. **C** is characterized by resistivity values going from 2034 Ωm to 6873 Ωm, it covers the distance along the profile of 10-90 m, 95-120 m, 140-170 m, 180-205 m, 240-270 m, and a depth/thickness of 2.5-12.8 m, 24.9 m, 12.8 m, 12.8 m and 18.5 m. However, zone **D** is portrayed by the resistivity of 6874 Ωm to 23241 Ωm, it located on 10-105 m, 115-155 m, 170-180 m, 200-245 m, and 270-290 m along the profile at a corresponding depth/thickness of 7.5-24.9 m, 7.5-24.9 m, 12.8 m, 24.9 m and 18.5 m respectively.

The subsurface variations for zones **A**, **B**, **C** and **D** in relation to Table 1, could be lateritic soil, highly decomposed schist, partially decomposed granite and quartzite, and quartzite/gneiss. However, low resistivity (zone **A**) in these regions could be because of water content as well as weathering in an oxidized rock. These rock types are basically of granite or rhyolite origin. As such, it could be associated with some minerals, especially gold. Zone **C** formed the dyke structures associated with partially decomposed granite and quartzite. These structures could play a pivotal role in determining the minerals, particularly gold mineralization. These results led to the development of the geologic section as given in Fig. 14(b).

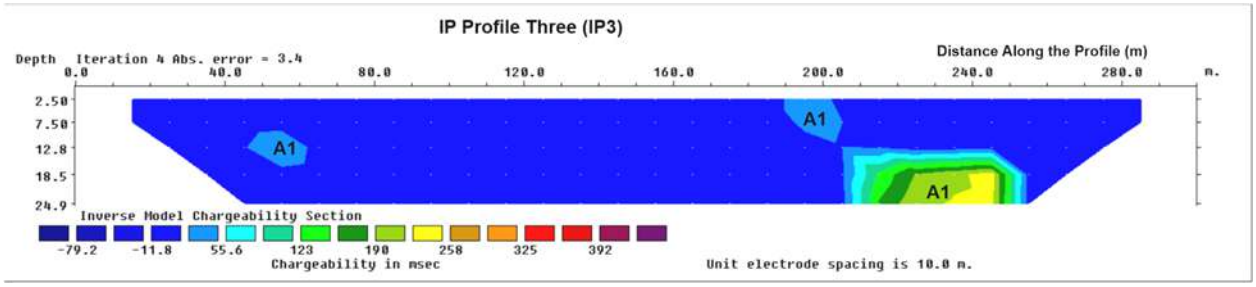

Fig 12. Inverse Model Chargeability Section for Profile Three (IP3)

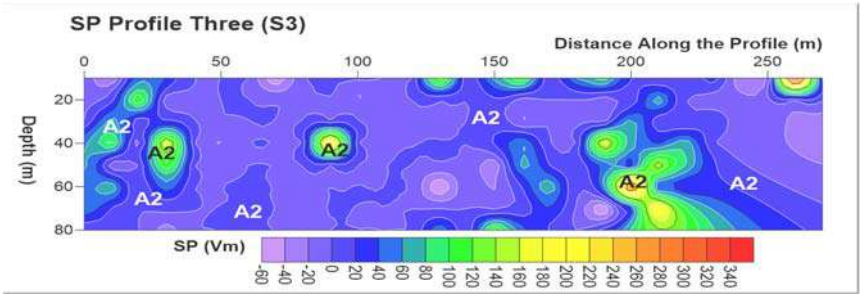

Fig. 13. SP 2D Section for Profile Three (S3)

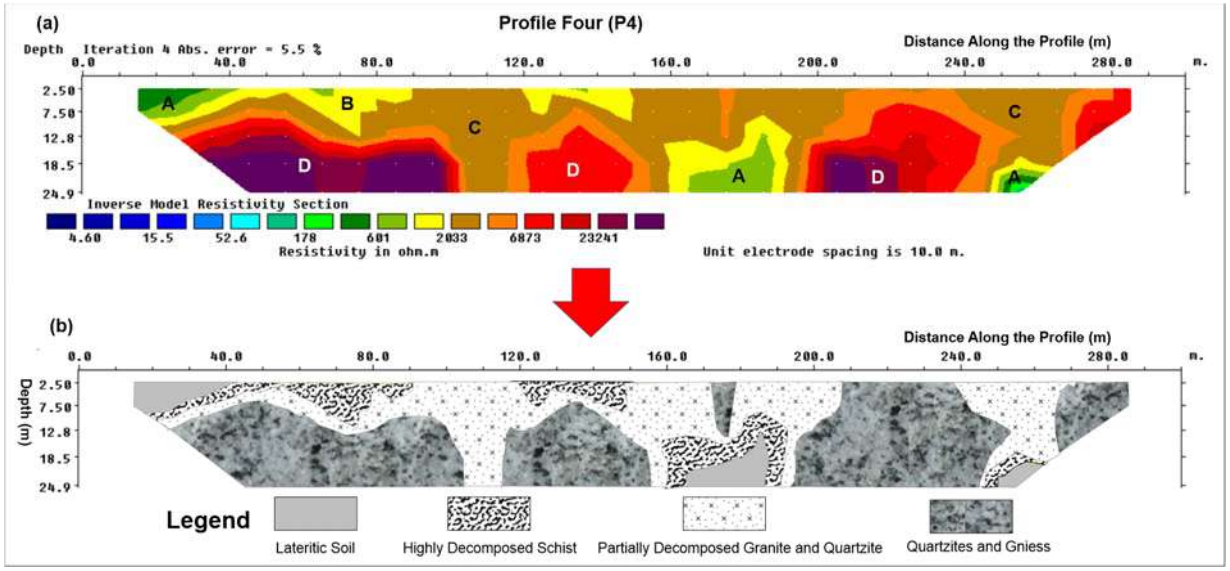

Fig. 14. (a) Inverse Model Resistivity Section and (b) Geologic Section for the Dataset along Profile Four (P4)

4.11 IP Model Section for Profile 4 (IP4)

Fig. 15 gives the results of the 2D inverse model chargeability section for profile four (IP4). The section uncovered some attributes of minerals, particularly within zone **A1**. The zones of **A1's** have the most imperative chargeability values ranging from 20 msec and above. It covers the lateral distance of 35-65 m, 55-80 m, 145-160 m, 200-220 m and 221-250 m at the corresponding depths of 12.8-24.9 m, 12.8 m, 18.5 m, 7.5 m and 7.5-24.9 m. Higher chargeability in zone **A1** is for the most part happening given an assortment of metallic minerals in host rocks. These areas could be considered as a potential target for the examination of explicit metallic minerals, particularly gold mineralization.

4.12 SP Section for Profile 4 (S4)

Fig. 16 gives the results of 2D SP sections along profile four (S4). The layer with high SP values (≥ 50 mV) was labeled as zone **A2.** It covers the lateral length of 1-40 m, 85-100 m, 145-200 m and 190-250 m, and a depth/thickness of 80 m, 22-60 m, 40 m and 80 m respectively. These regions with high SP values could occur due to either reduction-oxidation influence related to mineral bodies. These areas with high SP values were portrayed by vein-bearing metallic minerals. As such, the veins could be associated with gold mineralization in relation to the geological setting together with the borehole log of the area.

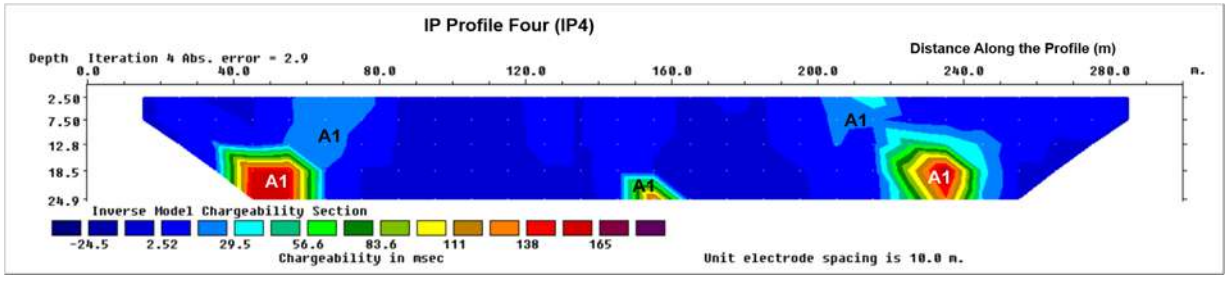

Fig. 15. Inverse Model Chargeability Section for Profile Four (IP4)

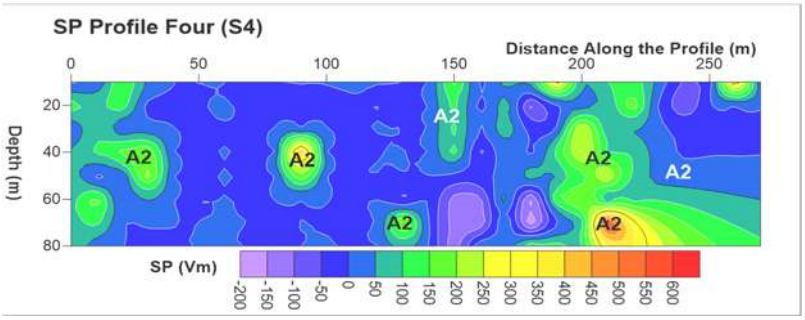

Fig. 16. SP 2D Section for Profile Four (S4)

4.13 Resistivity Model Section for Profile 5 (P5)

The 2D resistivity model section along profile five was given in Fig. 17(a). It covers a lateral distance of 300 m and lies between latitudes 10°47′42″N to 10°47′49.2″N and longitudes 4°44′56.4″E to 4°45′7.2″E (see Fig. 3). The subsurface resistivity signature was categorized as zones **A**, **B**, **C** and **D**. **A** is characterized by resistivity values ranging from 2.99 Ωm to 966 Ωm, it has occupied a length of 5-80 m, 90-105 m, 135-160 m, 170-190 m, 235-50 m and 270-290 m, and a depth/thickness of 7.5 m, 18.5-24.9 m, 7.5-18.5 m, 24.9 m, 18.5-24.9 m and 7.5 m respectively. **B** has resistivity values of 967 Ωm to 4095 Ωm, it covers a length of 10-90 m, 91-120 m, 145-180 m, 190-220 m and 240-270 m at a corresponding depth/thickness of 3-7.5 m, 18.5 m, 12.8 m, 24.9. m, and 18.5 m. **C** is characterized by resistivity values going from 4096 Ωm to 17353 Ωm, it covers the distance along the profile of 120-150 m, 160-175 m, 195-210 m, 220-240 m and 250-270 m, and a depth/thickness of 12.8 m, 18.5-24.9 m, 12.8-18.5 m, 19 m and 7.5-24.9 m respectively. However, zone **D** is portrayed by the resistivity of 17354 Ωm to 73547 Ωm, it has a length of 10-90 m, 110-170 m and 220-235 m at a corresponding depth/thickness of 7.5-24.9 m, 12.8-24.9 m and 12.8-18.5 m, respectively.

The suggested subsurface lithology for features **A**, **B**, **C**, and **D** from Table 1 could be lateritic soil, highly decomposed schist, partially decomposed granite and quartzite, and quartzite/gneiss. Zone **A** is associated with oxidized granite/quartzite and gneiss, and it could ordinarily be related to certain minerals, particularly gold. Zone **C** is also a potential zone for metallic minerals as it formed the dyke structures associated with partially decomposed granite and quartzite. These structures could play a pivotal role in determining the minerals, particularly gold mineralization. These results led to the development of the geologic section as given in Fig. 17(b).

4.14 IP Model Section for Profile 5 (IP5)

Fig. 18 revealed chargeability sections along profile five (IP5). The sections with high chargeability were labeled as zone **A1**. The zones cover a length of 30-45 m, 135-150 m, 140-170 m and 210-240 m and a depth/thickness of 7.5-18.5 m, 18.5-24.9 m, 2.5-18.5 m and 18.5 m respectively. Higher chargeability regions, **A1** (70 msec and above) could occur as a result of the existence of metallic minerals. These regions could be considered as an expected objective for the assessment unequivocal of gold mineralization.

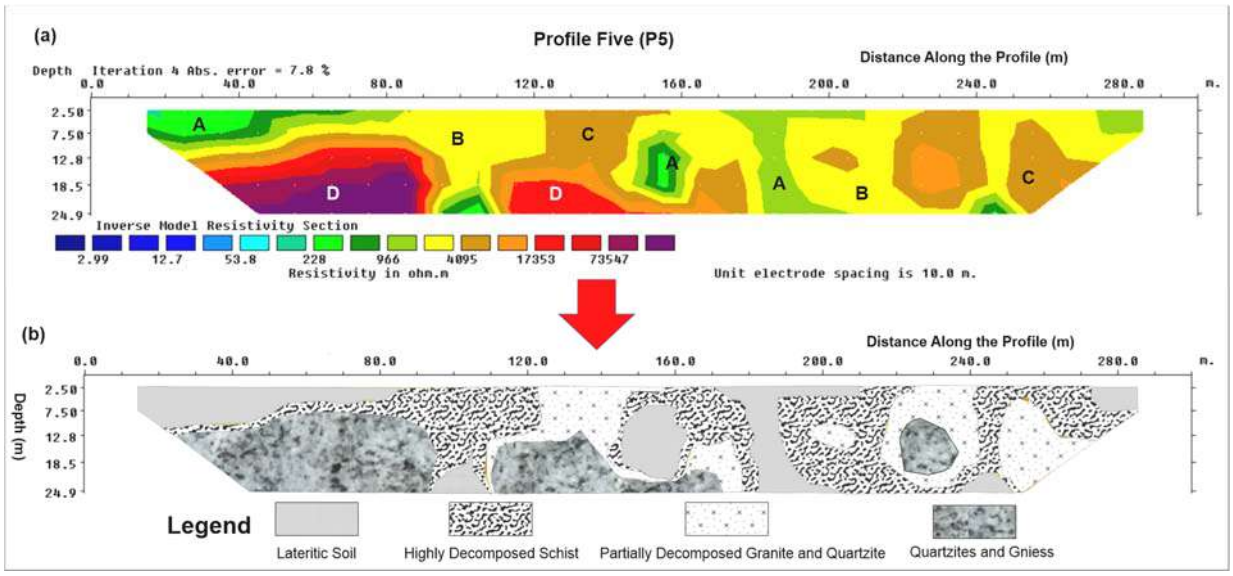

Fig. 17. (a) Inverse Model Resistivity Section and (b) Geologic Section for the Dataset along Profile Five (P5)

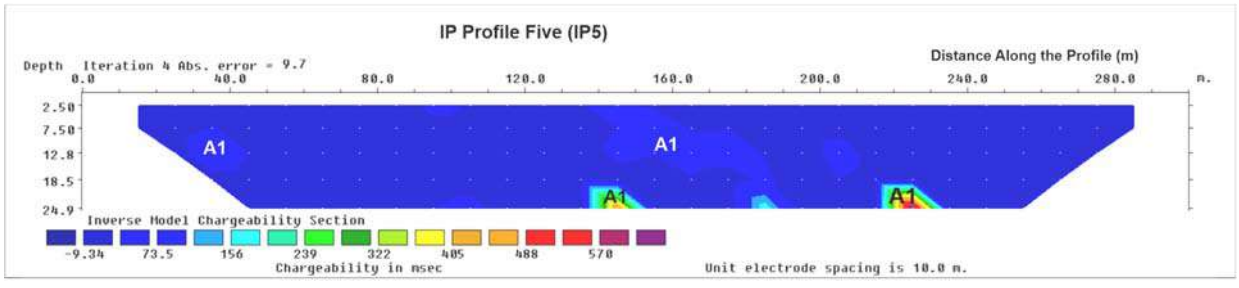

Fig. 18. Inverse Model Chargeability Section for Profile Five (IP5)

4.15 SP Section for Profile 5 (S5)

The results of 2D SP sections along profile five (S5) were given in Fig. 19. The section with high SP values (20 mV and above) was labeled as zone **A2**. These regions occupied a length of 60-80 m, 81-100 m and 140-180 m and a depth of 20-30 m, 45-64 m and 80 m respectively. These areas with high SP values were portrayed by vein-bearing metallic minerals. For that, the veins could be associated with gold mineralization related to the geological setting together with the borehole log of the area.

4.16 Resistivity Model Section for Profile 6 (P6)

Fig. 20(a) shows the 2D resistivity model section along profile six (P6). It is oriented in the NW-SE direction and covers a lateral extent of 300 m. The profile lies between latitudes 11°5′24″N to 11°5′34.8″N and longitudes 4°43′8.4″E to 4°43′19.2″E (see Fig. 3). The subsurface feature was sectionalized into zones **A**, **B**, **C** and **D**. Zone **A** is characterized by resistivity values ranging from 3.86 Ωm to 373 Ωm, it located on 5-45 m and 130-165 m, along the profile and a depth/thickness of 24.9 m and 18.5-24.9 m respectively. **B** has resistivity values of 374 Ωm to 1168 Ωm, it covers a length of 40-45 m, 130-165 m and 240-250 m at a corresponding depth/thickness of 24.9 m, 7.5-18.5 m and 12.8-18.5 m. **C** is characterized by resistivity values going from 41169 Ωm to 3664 Ωm, it covers the distance along the profile of 50-80 m, 120-150 m, 190-210 m and 230-270 m, and a depth/thickness of 24.9 m, 12.8 m, 18.5-24.9 m and 2.5-18.5 m. However, zone **D** is portrayed by the resistivity of 3665 Ωm to 11488 Ωm, it has a length of 50-60 m, 61-72 m, 80-130 m and 132-290 m at a corresponding depth/thickness of 12.8-24.9 m, 2.5-12.8 m, 24.9 m and 24.9 m.

The recommended subsurface lithology for highlights **A**, **B**, **C**, and **D** from Table 1 could be lateritic soil, highly decomposed schist, partially decomposed granite and quartzite, and quartzite/gneiss. Zone **A** is associated with oxidized granite/quartzite and gneiss, and it could ordinarily be related to certain minerals, particularly gold. **C** is also an expected zone for metallic minerals as it formed the dyke structures associated with partially decomposed granite and quartzite. These structures could play a pivotal role in determining the minerals, particularly gold mineralization. The result of the inverse model section given in Fig. 20(a) was further transformed into a geologic section as shown in Fig. 20(b).

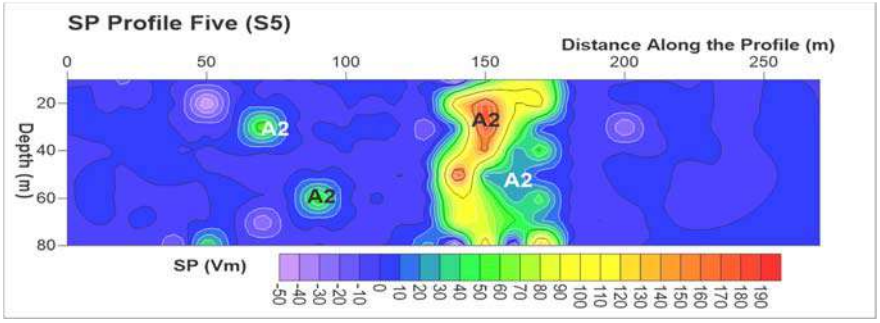

Fig. 19. SP 2D Section for Profile Five (S5)

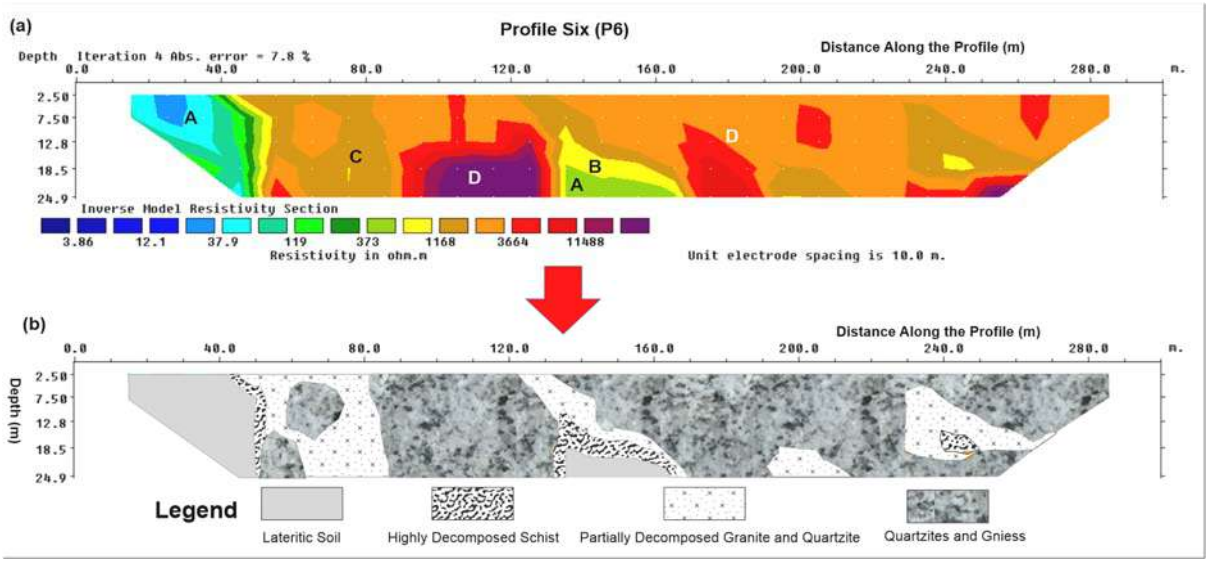

Fig. 20. (a) Inverse Model Resistivity Section and (b) Geologic Section for the Dataset along Profile Six (P6)

4.17 IP Model Section for Profile 6 (IP6)

2D chargeability section along profile six (IP6) was given in Fig. 21. The sections with high chargeability (≥ 20 msec) were labeled as zone **A1**. The zones occupied a length of 40-60 m, 75.5-120 m, 155-180 m and 200-220 m, and a depth/thickness of 12.8 m, 24.9 m, 24.9 m and 12.8 m respectively. Higher chargeability (zones **A1**) could occur as a result of the existence of metallic minerals. These regions could be considered as some of the expected areas for the exploration of gold mineralization.

4.18 SP Section for Profile 6 (S6)

The results of the 2D SP section along profile six (S6) were given in Fig. 22. The section with high SP values (≥20 mV) was labeled as zone **A2**. The zones A2's have a length of 0-50 m, 60-95 m, 110-140 m, 100-134 m, 150-190 m and 191-145 m and a depth/thickness of 80 m, 80 m, 44 m, 60-80 m, 80 m and 20-80 m respectively. The regions of high SP values were portrayed by vein-bearing metallic minerals. These veins could be associated with gold mineralization as compared with the geological setting coupled with the borehole log of the area.

4.2.19 Resistivity Model Section for Profile 7 (P7)

Profile 7 covers a lateral extent of 300 m (Fig. 23a). It is oriented in the NW-SE direction and lies between latitudes 11°5′16.8″N to 11°5′24″N and longitudes 4°43′15.6″E to 4°43′4.8″E (see Figure 3). The subsurface features from Fig. 23(a) could be sectionalized into four: **A**, **B**, **C**, and **D**. Zone **A** is characterized by low resistivity values ranging from 17.5 Ωm to 376 Ωm, it is located on 10-30 m, 45-70 m, 90-120 m, 160-200 m and 250-270 m distance along the profile at a corresponding depth/thickness of 2.5-18.5 m, 7.5-18.5 m, 7.5-18.5 m, 12.8-24.9 m and 7.5-18.5 m respectively. Zone **B** has resistivity features of 377 Ωm to 2912 Ωm, it has a length of 50-90 m and 60-105 m, and a depth/thickness of 12.8 m, 18.5 m and 12.8 m respectively. **C** is characterized by resistivity values ranging from 2913 Ωm to 8099 Ωm, it covers the distance along the profile from 10-40 m, 150-160 m, 190-235 m and 250-290 m and a depth/thickness of 12.8 m, 2.5 m, 12.8 m and 7.5 m respectively. However, zone **D** is characterized by the resistivity of 8100 Ωm to 22527 Ωm, it has a length of 45-90 m, 80-125 m, 00-150 m, and 200-240 m and a depth/thickness of 12.8-24.9 m, 7.5 m, 12.8-24.9 m, and 12.8-24.9 m respectively.

The suggested subsurface lithology for features **A**, **B**, **C**, and **D** from Table 1 could be lateritic soil, highly decomposed schist, partially decomposed granite and quartzite, and quartzite/gneiss. However, low resistivity regions of zone **A** could be a result of water content and weathering in the oxidized rock. Some minerals, particularly gold, could be hosted mostly in a rock corroded by water called oxidized rocks, mainly of granite or rhyolite origin. Zone **C** of partially decomposed granite and quartzite has formed the dyke structures. Dyke subsurface structures of decomposed granite and quartzite usually play a pivotal role in determining the gold mineral. The results of the inverse model section (Fig. 23a) were indicated in the geologic section as given in Fig. 23(b).

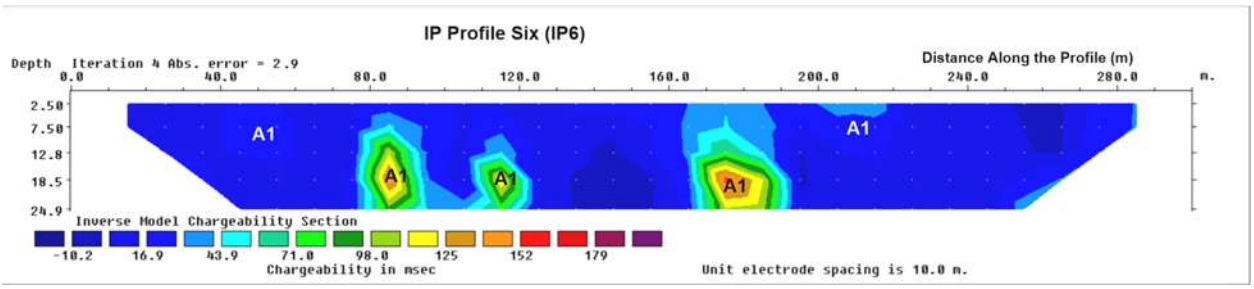

Fig. 21. Inverse Model Chargeability Section for Profile Six (IP6)

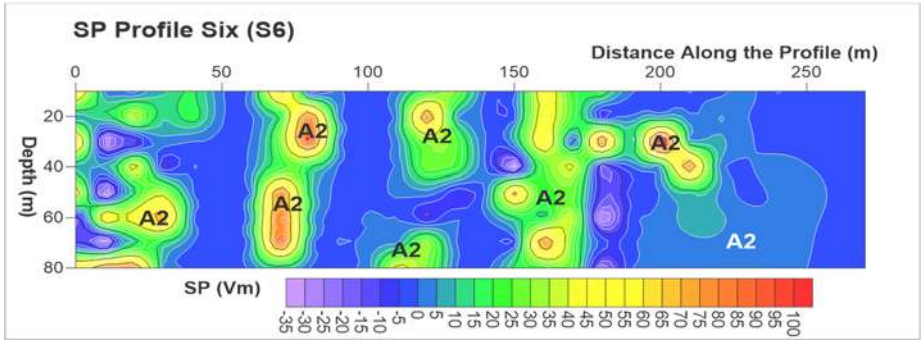

Fig. 22. SP 2D Section for Profile Six (S6)

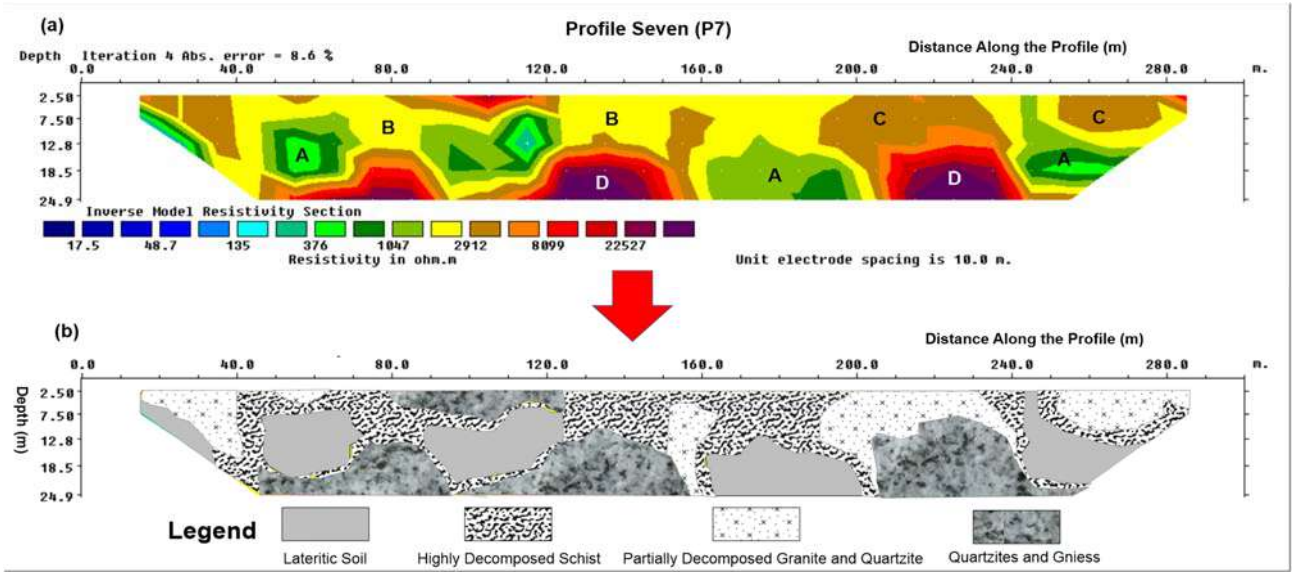

Fig. 23. (a) Inverse Model Resistivity Section and (b) Geologic Section for the Dataset along Profile Seven (P7)

4.2.20 IP Model Section for Profile 7 (IP7)

The 2D chargeability section along profile seven (IP7) was given in Fig. 24. It revealed the zone of high SP values (≥ 61 msec), was labeled as zone **A1.** The zones **A1** cover the lateral extent of 1-60 m, 62-80 m, 70-130 m, 150-190 m, 192-260 m and 265-300 m and a depth/thickness of 24.9 m, 18.5-24.9 m, 24.9 m, 24.9 m,18.5 m and 18.5 m respectively. Higher chargeability regions (zones **A1)** could be considered as an assortment of metallic minerals that could usually occur in a host rock. These areas could be considered potential zones of metallic minerals, particularly gold mineralization.

4.2.21 SP Section for Profile 7 (S7)

Fig. 25 gives the results of 2D SP segments along profile seven (S7). The section with high SP values (≥ 20 mV) was labeled as zone **A2**. It has a length of 1-48 m, 60-125 m, 130-175 m and 200-300 m, and a depth/thickness of 60 m, 80 m, 80 m and 60 m respectively. These regions could be considered as the areas depicted by vein-bearing metallic minerals, such as gold minerals.

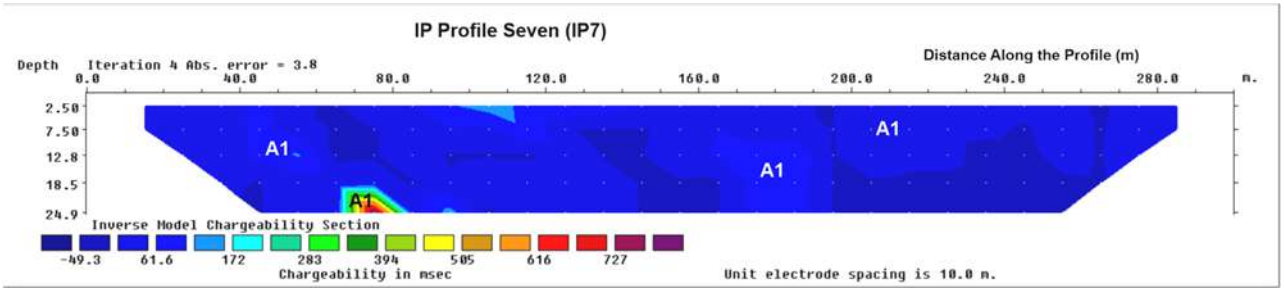

Fig. 24. Inverse Model Chargeability Section for Profile Seven (IP7)

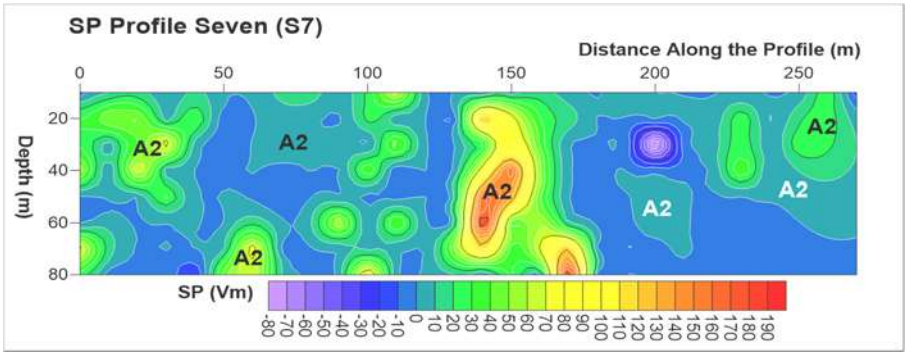

Fig. 25. SP 2D Section for Profile Seven (S7)

Table 2

Summary of results obtained from the integrated methods

Profile	Resistivity Results				Induced polarization Results				Self-Potential Results				Probable gold mineralization potential remarks
	Zone	Resistivity ranges (Ωm)	Lateral lengths (m)	Depth/ Thickness (m)	Zone	Chargeability ranges (msec)	Lateral lengths (m)	Depth/ Thickness (m)	Zone	SP ranges (mV)	Lateral lengths (m)	Depth/ Thickness (m)	
P1	A	117 to 944	5-45, 55-102, 145-165, and 241-285	19, 19-24.9, 19 and 17-24.9	A1	38.4 to 290	120-140, 170-190, 230-260 and 205-290	18.5-24, 12.8, 18.5 and 24.9	A2	20 and above	0-10 55-75 and 120-140	50, 80, and 40	Yes
	B	945 to 7638	50-90 and 60-105	13 and 18.5-20	-	-	-	-	-	-	-	-	No
	C	7639 to 21728	90-165	18.5	-	-	-	-	-	-	-	-	Yes
	D	61815 to 175857	90-140 and 160-250	7.5-24.9 and 24.9	-	-	-	-	-	-	-	-	No
P2	A	113 to 594	10-30, 160-165 and 202-222	12, 24.9 and 2.5	A1	35 and above	35-60, 50-85, 140-175, 110-195, 198-220 and 230-250	12.8-24.9, 12.8, 12.8-24.9, 12.8, 7.5 and 18.5	A2	20 and above	0-54, 50-60, 61-100, 145-155, 160-210 and 115-140	80, 80, 20-65, 40 m, 60, and 80	Yes
	B	1359 to 3112	12-41, 50-80, 110-160, 169-230. 231-249 and 270-285	24.9, 24.9, 12.8, 18.5, 24.9, and 18.5	-	-	-	-	-	-	-	-	No
	C	3113 to 7123	41-50 and 81-120	each 18.5	-	-	-	-	-	-	-	-	Yes
	D	7124 to 37331	41-70, 50-80, 110-160, 169-230, 170-220, 231-249, and 270-285	12-24.9, 7.5-12, 12-24.9, 13.0-24.9 and 250-270	-	-	-	-	-	-	-	-	No
P3	A	1.6 to 459	10-80, 190-200 and 250-265.	12.0, 18.5-24.9 and 7.5-18.5	A1	≥ 20	45-60, 190-202 and 202-255	7.5-18.5, 7.5 and 12.8-24.9	A2	≥ 40	0-40, 50-60, 70-100, 120-200, 140-135, 190-240	70, 21, 21-41, 15, 80 and 21-80	Yes
	B	460 to 1888	30-110, 130-149, 190-200 and 245-265	2.5-18.5, 24.9, 18.5 and 2.5-18.5	-	-	-	-	-	-	-	-	No
	C	1889 to 7773	35-55, 70-92, 105-130, 145-180, 200-210 and 220-270	8-24.9, 3-24.9, 24.9, 24.8, 24.9 and 7.5	-	-	-	-	-	-	-	-	Yes
	D	7774 to 32002	100-125, 175-190, 200-250 and 265-290	7.5-24.9, 12-24.9, 2.5-24.9 and 18.5	-	-	-	-	-	-	-	-	No
P4	A	4.6 to 601	5-40, 165-185, 245-260	7.5, 18.5-24.9 and 18.5-24.9	A1	20 and above	35-65, 55-80, 145-160, 200-220 and 221-250	12.8-24.9, 12.8, 18.5, 7.5 and 7.5-24.9	A2	≥50	1-40, 85-100, 145-200 and 190-250	80, 22-60, 40 and 80	Yes

Profile	Resistivity Results				Induced polarization Results				Self-Potential Results				Probable gold mineralization potential remarks
	Zone	Resistivity ranges (Ωm)	Lateral lengths (m)	Depth/ Thickness (m)	Zone	Chargeability ranges (msec)	Lateral lengths (m)	Depth/ Thickness (m)	Zone	SP ranges (mV)	Lateral lengths (m)	Depth/ Thickness (m)	
	B	602 to 2033	40-90, 120-150, and 155-190	12, 7.5 and 18.5-24.9	-	-	-	-	-	-	-	-	No
	C	2034 to 6873	10-90, 95-120, 140-170, 180-205, 240-270	2.5-12.8, 24.9, 12.8, 12.8 and 18.5	-	-	-	-	-	-	-	-	Yes
	D	6874 to 23241	10-105, 115-155, 170-180, 200-245, and 270-290	7.5-24.9, 7.5-24.9, 12.8, 24.9 and 18.5	-	-	-	-	-	-	-	-	No
P5	A	2.99 to 966	5-80, 90-105, 135-160, 170-190, 235-50 and 270-290	7.5, 18.5-24.9, 7.5-18.5, 24.9, 18.5-24.9 and 7.5	A1	70 and above	30-45, 135-150, 140-170 and 210-240	7.5-18.5, 18.5-24.9, 2.5-18.5 and 18.5	A2	20 and above	60-80, 81-100 and 140-180	20-30, 45-64 and 80	Yes
	B	967 to 4095	10-90, 91-120, 145-180, 190-220 and 240-270	3-7.5, 18.5, 12.8, 24.9, and 18.5	-	-	-	-	-	-	-	-	No
	C	4096 to 17353	120-150, 160-175, 195-210, 220-240 and 250-270	12.8, 18.5-24.9, 12.8-18.5, 19 and 7.5-24.9	-	-	-	-	-	-	-	-	Yes
	D	17354 to 73547	10-90, 110-170 and 220-235	7.5-24.9, 12.8-24.9 and 12.8-18.5	-	-	-	-	-	-	-	-	No
P6	A	3.86 to 373	5-45 and 130-165	24.9 and 18.5-24.9	A1	≥ 20	40-60, 75.5-120, 155-180 and 200-220	12.8, 24.9, 24.9 and 12.8	A2	≥20	0-50, 60-95, 110-140, 100-134, 150-190 and 191-145	80, 80, 44, 60-80, 80 and 20-80	Yes
	B	374 to 1168	40-45, 130-165 and 240-250	24.9, 7.5-18.5 and 12.8-18.5	-	-	-	-	-	-	-	-	No
	C	41169 to 3664	50-80, 120-150, 190-210 and 230-270	24.9, 12.8, 18.5-24.9 and 2.5-18.5	-	-	-	-	-	-	-	-	Yes
	D	3665 to 11488	50-60, 61-72, 80-130 and 132-290	12.8-24.9, 2.5-12.8, 24.9, 24.9	-	-	-	-	-	-	-	-	No
P7	A	17.5 to 376	10-30, 45-70, 90-120, 160-200 and 250-270	2.5-18.5, 7.5-18.5, 7.5-18.5, 12.8-24.9 and 7.5-18.5	A1	≥ 61	1-60, 62-80, 70-130, 150-190, 192-260 and 265-300	24.9, 18.5-24.9, 24.9, 24.9, 18.5 and 18.5	A2	≥ 20	1-48, 60-125, 130-175 and 200-300	60, 80, 80 and 60	Yes
	B	377 to 2912	50-90 and 60-105	12.8, 18.5 and 12.8	-	-	-	-	-	-	-	-	No
	C	2913 to 8099	10-40, 150-160, 190-235 and 250-290	12.8, 2.5, 12.8 and 7.5	-	-	-	-	-	-	-	-	Yes
	D	8100 to 22527	45-90, 80-125, 00-150, and 200-240	12.8-24.9, 7.5, 12.8-24.9, 12.8-24.9	-	-	-	-	-	-	-	-	No

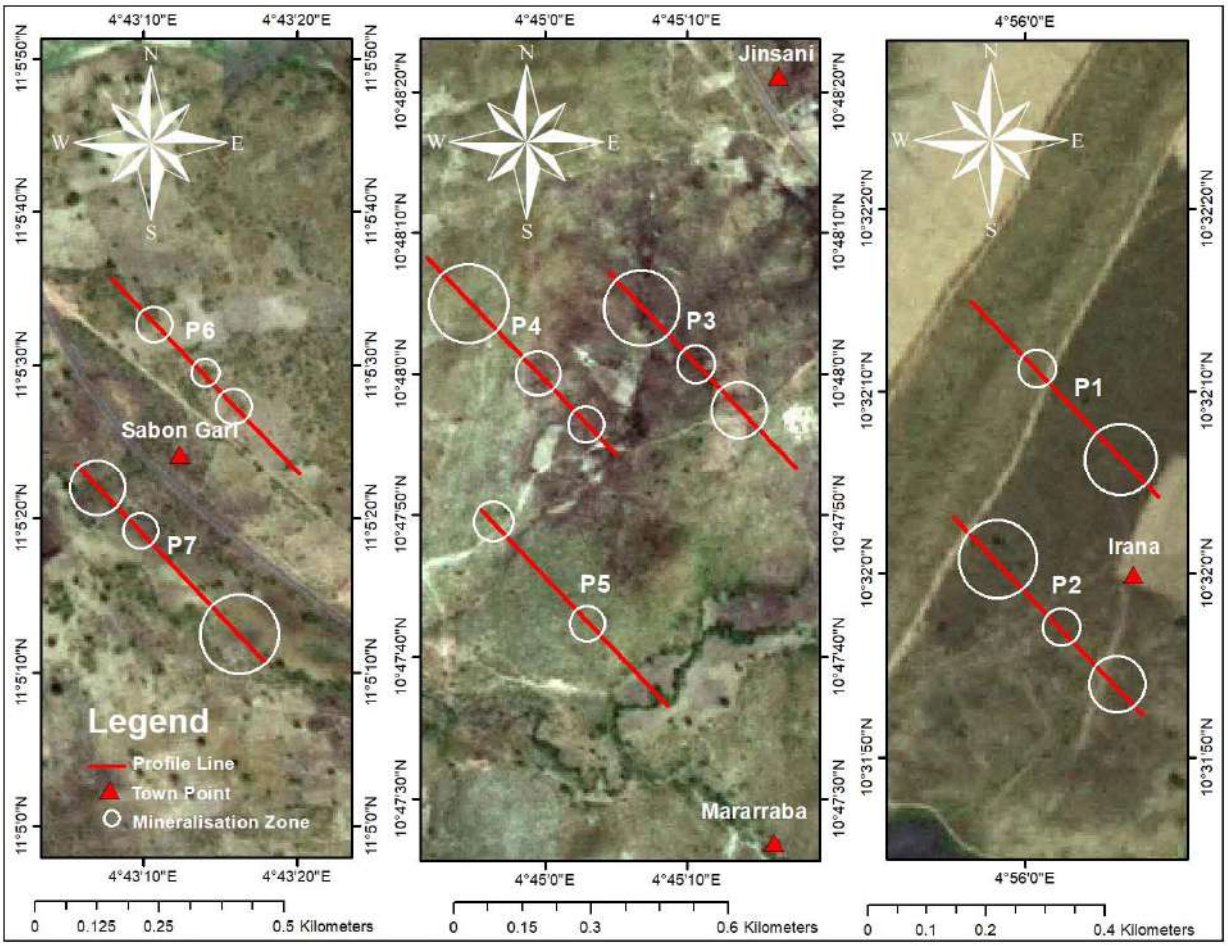

Fig. 26. Potential mineralization zones of the study areas

5. Discussion

5.1 Integrated results for profile one

The zones of potential mineralization were revealed within the regions of low (117 Ωm to 944 Ωm) and high (61815 Ωm to 175857 Ωm) resistivity in the resistivity cross sections along profile one (Fig. 5). Low resistivity anomalous areas (zones **A**) were corresponding to oxidized rock. These rock types are corroded by water and were mainly of granite or rhyolite origin. These regions could generally be associated with explicit minerals, particularly gold, while the regions with high resistivity signatures (zone **C**) formed dyke structures. These structures were associated with partially decomposed granite and quartzite as compared with the geological setting/borehole log of the area.

However, these zones for potential mineralization occurred within the zones of high chargeability of ≥ 20 msec in the IP cross sections (see Fig. 6), as well as occurred in the regions of high SP anomalies of 20 mV and above (Fig. 7). These areas revealed the presence of sulphide-containing gold.

The major zones of mineral potentials are located between 120-140 m and 230-290 m with a corresponding depth of 24.9 m each. These regions are **A** and **C** (Fig. 5), **A1** (Fig. 6) and **A2** (Fig. 7) of the low/or high resistivity, high chargeability and high SP values. The zones could be inferred to contain traces of minerals in their respective host rocks. These regions could be considered as a potential target for the exploration of metallic minerals such as gold mineralization. These areas corresponded to the northern part of Irana of Niger state (see Fig. 26).

5.2 Integrated results for profile two

Profile two shows the suggested zones of mineralization potential to occur at zones **A** and **C**, **A1** and **A2**. These zones were the areas of low/or high resistivity (zones **A** and **C**), high chargeability **A1**), and high SP (**A2**) anomalous as shown in Fig's 8, 9 and 10. The major zones of mineral potentials are suggested to be between 35-62 m, 41-120 m, 145-165 m and 202-240 m with a corresponding depth of 24.9 m, 18.5 m, 24.9 m and 18.5 m. The zones could be inferred to contain traces of minerals in their respective host rocks. These areas could be considered as a possible target for the exploration of metallic minerals, particularly, gold minerals. These regions corresponded to the SW part of Irana of Niger state (Fig. 26).

5.3 Integrated results for profile three

The suggested zones of mineralization potential along profile three are zone **A** and **C**, **A1** and **A2**. These regions are characterized by low/high resistivity, high chargeability and high SP anomalous (Fig's 11, 12 and 14). The major zones of mineral potentials are suggested to be between 10-80 m, 190-200 m and 202-255 m with a corresponding depth of 18.5 m, 24.9 m and 24.9 m. The zones could be inferred as a potential target for the exploration of metallic minerals, particularly gold mineralization. These areas corresponded to the northern part of Mararraba and SW of Jinsani areas of Kebbi state (Fig. 26).

5.4 Integrated results for profile four

Profile four shows the suggested zones of mineralization potential to occur at zone **A** and **C**, **A1** and **A2**. These zones were the areas of low/or high resistivity (zones **A** and **C**), high chargeability **A1**), and high SP (**A2**) anomalous as shown in Fig's 14, 15 and 16. The major zones of mineral potentials are suggested to be between 35-100 m, 145-200 m and 220-250 m with a corresponding depth of 12.8 m, 18.5 m and 24.9 m. The zones could be inferred to contain traces of minerals in their respective host rocks. These areas could be considered as a possible target for the exploration of metallic minerals, particularly gold minerals. These regions corresponded to the NW part of Mararraba and SW of Jinsani areas of Kebbi state (Fig. 26).

5.5 Integrated results for profile five

The suggested zones of mineral potential occurred at zones **A** and **C** (Fig. 17), **A1** (Fig. 18) and **A2** (Fig. 19). The zones were characterized by low/high resistivity, high chargeability and high SP anomalous. The integrated zones of mineral potentials are suggested to be between 0-45 m and 140-180 m with a corresponding depth of 18.5 m and 28.5 m. The zones could be inferred as a potential target for the exploration of metallic minerals, particularly gold mineralization. These regions corresponded to the NW part of the Mararraba area of Kebbi state (Fig. 26).

5.6 Integrated results for profile six

For profile six, the suggested zone for mineral trapping structure/ or mineralization potential was named zone **A&C**, **A1** and **A2** (Fig's 20, 21&22). The critical zones for mineralization prospects were found to be between 60-95 m, 110-140 m and 150-190 m at a corresponding depth of 7.5-60 m, 18.5-40 m and 2.5-80 m. These regions could be considered a potential target area for assessing metallic minerals, particularly gold mineralization. These zones corresponded to the northern part of the Sabon Gari area of Kebbi state (Fig. 26).

5.7 Integrated results for profile seven

The suggested zones of mineral potential occurred at zones **A&C** (Fig. 23), **A1** (Fig. 24) and **A2** (Fig. 25). The zones were characterized by low/high resistivity, high chargeability and high SP anomalous. The integrated zones of mineral potentials are suggested to be between 1-60 m, 130-170 m and 200-300 m with a corresponding depth of 45 m, 2.5-7.5 m and 18.5 m. The zones could be inferred as a potential target for the exploration of metallic minerals, particularly gold mineralization. These regions corresponded to the southern part of the Sabon Gari area of Kebbi state (Fig. 26).

6. Conclusions

Integrated 2D geoelectric prospecting methods involves of ERT, IP and SP techniques were employed as a follow-up details geophysical survey tools on the anomalous zones detected from the aeromagnetic studied by Authors: Augie et al. (2021b), (2022b) and (2022c). The anomalous detected by earlier studies conducted by the aforementioned Author revealed the major structures (lineament) associated with mineralization potential which could play an important role in gold exploration and exploitation in the area. These areas were found to be SE parts of Yauri and Shanga, Fakai, Ngaski, Zuru, Magama, Rijau, Eastern part of Wasagu/Danko and Bukkuyum. However, this study details a geophysical survey conducted at Yauri (Jinsani and Mararraba), Shanga (Sabon Gari) and Magama (Irana). A total of 7 profiles were designed using a dipole-pole configuration with each 300 m distance along the profile. Profiles 1 and 2 were conducted at Magama (Irana), profiles 3 and 4 at Shanga (Sabon Gari) and profiles 5, 6 and 7 at Yauri (Jinsani and Mararraba).

The results of profiles 1, 2, 3, 4, 5, 6 and 7 revealed the region's low/or high resistivity, high chargeability and high SP values that were inferred as zones for mineral potential. Low resistivity anomalous (zones **A**) corresponds to oxidised rocks associated with granite/quartzite veins. The regions with high resistivity signatures (zones **C**) formed dyke structures associated with partially decomposed granite and quartzite as compared with the geological setting and the borehole log of the area. These zones for potential mineralization coincided with the zones of high chargeability (≥ 20 msec) in the IP cross sections as well as the regions of high SP anomalies (20 mV and above).

The major zones of mineral potentials found in this study along the integrated profile one P1 are to be 35-62 m, 41-120 m, 145-165 m and 202-240 m at a corresponding depth/thickness of 24.9 m, 18.5 m, 24.9 m and 18.5 m. Potential mineralized zone for profile two P2 lies between 35-62 m, 41-120 m, 145-

165 m and 202-240 m at a corresponding depth of 24.9 m, 18.5 m, 24.9 m and 18.5 m. Likewise, P3 has a length of 10-80 m, 190-200 m and 202-255 m, and a depth/thickness of 18.5 m, 24.9 m and 24.9 m. Integrated profile four also revealed the lateral extent of 35-100 m, 145-200 m and 220-250 m at a corresponding depth/thickness of 12.8 m, 18.5 m and 24.9 m. P5 also is between 0-45 m and 140-180 m at a corresponding depth/thickness of 18.5 m and 28.5 m. P6 has a length of 60-95 m, 110-140 m and 150-190 m and it has a depth/thickness of 7.5-60 m, 18.5-40 m and 2.5-80 m respectively. And P4 reveals the lateral extent of 1-60 m, 130-170 m and 200-300 m with a corresponding depth of 45 m, 2.5-7.5 m and 18.5 m. These regions could be considered as a possible pathway for gold exploration and exploitation. These areas corresponded to the northern part of Irana, the SW part of Irana, the northern part of Mararraba, the NW part of Marrarba, the SW part of Jinsani, and the northern part of Sabon Gari and the southern part of Sabon Gari areas of Niger and Kebbi state.

Acknowledgements

The authors are grateful to the Tertiary Education Fund (Tetfund) for funding this research.

Thanks to the district heads of Mararraba, Sabon Gari and Irana of Kebbi and Niger states for approval and for facilitating geophysical data collection. Their appreciation also goes to the department of Physics, Bayero University Kano and the department of Geophysics, Federal University of Technology Minna for providing the instruments.

REFERENCES

Amoah B.K., Dadzie I., Takyi-kyeremeh K. Integrating gravity and magnetic field data to delineate structurally controlled gold mineralization in the Sefwi Belt of Ghana. Journal of Geophysics and Engineering, Vol. 15, No. 4, 2018, pp. 1197-1203, https://doi.org/10.1088/1742-2140/aaa7b2.

Augie A.I. and Ridwan M.M. Delineation of potential mineral zones from aeromagnetic data over eastern part of Zamfara. Savanna Journal of Basic and Applied Sciences, Vol. 3, No.1, 2021, pp. 60-66.

Augie A.I. and Sani A.A. Interpretation of aeromagnetic data for gold mineralization potential over Kabo and its environs NW Nigeria. Savanna Journal of Basic and Applied Sciences, Vol. 2, No. 2, 2020, pp. 116-123.

Augie A.I., Adamu A., Salako K.A., Alkali A., Narimi A.M., Yahaya M.N., Sani A.A. Assessment for gold mineralization potential over Anka schist belts NW Nigeria using aeromagnetic data. FUDMA Journal of Sciences (FJS), Vol. 5, No. 4, 2021a, pp. 235-242.

Augie A.I., Salako K.A., Rafiu A.A., Jimoh M.O. Estimation of depth to structures associated with gold mineralization potential over southern part of Kebbi state using aeromagnetic data. 3rd School of Physical Sciences Biennial International Conference Futminna 2021, Federal University of Technology Minna, 2021b, pp. 290-297.

Augie A.I., Salako K.A., Rafiu A.A., Jimoh M.O. Geophysical assessment for gold mineralization potential over the southern part of Kebbi state using aeromagnetic data. Geology, Geophysics and Environment, Vol. 48, No. 2, 2022b, pp. 177-193, https://doi.org/10.7494/geol.2022.48.2.177.

Augie A.I., Salako K.A., Rafiu A.A., Jimoh M.O. Geophysical magnetic data analyses of the geological structures with mineralization potentials over the southern part of Kebbi, NW Nigeria. Mining Science, Vol. 29, 2022c, pp. 179-203, https://doi.org/10.37190/msc222911.

Augie A.I., Saleh M., Ologe O., Salako K.A., Rafiu A.A., Yahaya M.N. Correlation of 2D electrical resistivity and self-potential methods for the assessment of the integrity of Goronyo dam NW Nigeria. Chiang Mai University Journal of Natural Sciences, Vol. 21, No. 3, 2022a, e2022043, https://doi.org/ 10.12982/CMUJNS.2022.043.

Bagare A.A., Saleh M., Aku M.O., Abdullahi Y.M. 2D electrical study to delineate subsurface structures and potential mineral zones at Alajawa artisanal mining site Kano state Nigeria. Journal of the Nigerian Geophysical Society, Vol. 1, No. 1, 2018, pp. 24-32.

ЛИТЕРАТУРА

Amoah B.K., Dadzie I., Takyi-kyeremeh K. Integrating gravity and magnetic field data to delineate structurally controlled gold mineralization in the Sefwi Belt of Ghana. Journal of Geophysics and Engineering, Vol. 15, No. 4, 2018, pp. 1197-1203, https://doi.org/10.1088/1742-2140/aaa7b2.

Augie A.I. and Ridwan M.M. Delineation of potential mineral zones from aeromagnetic data over eastern part of Zamfara. Savanna Journal of Basic and Applied Sciences, Vol. 3, No.1, 2021, pp. 60-66.

Augie A.I. and Sani A.A. Interpretation of aeromagnetic data for gold mineralization potential over Kabo and its environs NW Nigeria. Savanna Journal of Basic and Applied Sciences, Vol. 2, No. 2, 2020, pp. 116-123.

Augie A.I., Adamu A., Salako K.A., Alkali A., Narimi A.M., Yahaya M.N., Sani A.A. Assessment for gold mineralization potential over Anka schist belts NW Nigeria using aeromagnetic data. FUDMA Journal of Sciences (FJS), Vol. 5, No. 4, 2021a, pp. 235-242.

Augie A.I., Salako K.A., Rafiu A.A., Jimoh M.O. Estimation of depth to structures associated with gold mineralization potential over southern part of Kebbi state using aeromagnetic data. 3rd School of Physical Sciences Biennial International Conference Futminna 2021, Federal University of Technology Minna, 2021b, pp. 290-297.

Augie A.I., Salako K.A., Rafiu A.A., Jimoh M.O. Geophysical assessment for gold mineralization potential over the southern part of Kebbi state using aeromagnetic data. Geology, Geophysics and Environment, Vol. 48, No. 2, 2022b, pp. 177-193, https://doi.org/10.7494/geol.2022.48.2.177.

Augie A.I., Salako K.A., Rafiu A.A., Jimoh M.O. Geophysical magnetic data analyses of the geological structures with mineralization potentials over the southern part of Kebbi, NW Nigeria. Mining Science, Vol. 29, 2022c, pp. 179-203, https://doi.org/10.37190/msc222911.

Augie A.I., Saleh M., Ologe O., Salako K.A., Rafiu A.A., Yahaya M.N. Correlation of 2D electrical resistivity and self-potential methods for the assessment of the integrity of Goronyo dam NW Nigeria. Chiang Mai University Journal of Natural Sciences, Vol. 21, No. 3, 2022a, e2022043, https://doi.org/ 10.12982/CMUJNS.2022.043.

Bagare A.A., Saleh M., Aku M.O., Abdullahi Y.M. 2D electrical study to delineate subsurface structures and potential mineral zones at Alajawa artisanal mining site Kano state Nigeria. Journal of the Nigerian Geophysical Society, Vol. 1, No. 1, 2018, pp. 24-32.

Bonde D.S., Lawali S., Salako K.A. Structural mapping of solid mineral potential zones over southern part of Kebbi state, northwestern Nigeria. Journal of Scientific and Engineering Research, Vol. 6, No. 7, 2019, pp. 229-240.

Dahlin T., Zhou B. A numerical comparison of 2D resistivity imaging with 10 electrode arrays. Geophysical Prospecting, Vol. 52, 2004, pp. 379-398.

Danbatta U.A. Precambrian crustal development in the northwestern part of Zuru schist belt, northwestern Nigeria. Journal of Mining and Geology, Vol. 44, No. 1, 2008, pp. 43-56.

Danbatta U.A. Precambrian crustal development of the northwestern part of Zuru schist belt, NW Nigeria. A paper presented at the 41st annual conference of Nigerian mining, and geosciences society (NMGS), 2005, Abstr., p. 13.

Danjumma S.G., Bonde D.S., Mohammed A., Lawali S., Birnin Tudu A.M. Identification of mineral deposits in Garin Awwal mining site, Kebbi state, north-western Nigeria. Journal of Multidisciplinary Engineering Science and Technology (JMEST), Vol. 6, No. 6, 2019, pp. 10276-10280.

Ejepu J.S., Unuevho C.I., Agbor A.T., Abdullahi S. Integrated geosciences prospecting for gold mineralization in Kwakuti north-central Nigeria. Journal of Geology and Mining, Vol. 10, No. 7, 2018, pp. 81-94, https://doi.org/10.5897/JGMR 2018.0296.

Fedi M. and Abbas M.A. A fast interpretation of self-potential data using the depth from extreme points method. Geophysics, Vol. 78, No. 2, 2012, pp. 107-116.

Jamaluddeen S.S., Bunawa A.A., Saleh M. An assessment of the groundwater potential of Bayero University Kano Permanent Site using induced polarization and self-potential methods. Journal of Earth science and Engineering, Vol. 4, 2014, pp. 587-596.

Lawal M.M., Salako K.A., Abbas M., Adewumi T., Augie A.I., Khita M. Geophysical investigation of possible gold mineralization potential zones using a combined airborne magnetic data of lower Sokoto basin and its environs northwestern Nigeria. International Journal of Progressive Sciences and Technologies (IJPSAT), Vol. 30, No. 1, 2021, pp. 01-16.

Lawali S., Salako K.A., Bonde D.S. Delineation of mineral potential zones over lower part of Sokoto basin, northwestern Nigeria using aeromagnetic data. Academic Research International, Vol. 11, No. 2, 2020, pp. 19-29.

Lobo-Guerrero A. Application of spontaneous potential profiles for exploration of gold-rich epithermal low sulphidation veins in a humid region. Geoscience Africa 2004, Conference organized by the Geological Society of South Africa in Johannesburg, University of the Witwatersrand, Johannesburg, 2004.

Loke H.M. and Barker R.D. Rapid least-square inversion of apparent resistivity pseudosections. Geophysical Prospecting, Vol. 44(1), 1996, pp. 131-152**,** DOI:10.1111/j.1365-2478. 1996.tb00142.x.

Loke H.M. Tutorial: 2-D and 3-D electrical imaging surveys. Revised edition; 26th July 2004, 128 p.

Oduduru P.I. and Mamah L.I. Integration of electrical resistivity and induced polarization for subsurface imaging around Ihe pond, Nsukka, Anambra basin, Nigeria. Pacific Journal of Science and Technology, Vol. 15, No. 1, 2014, pp. 306-317.

Olalekan O., Afees O., Ayodele S. An Empirical analysis of the contribution of mining sector to economic development in Nigeria. Khazar Journal of Humanities and Social Sciences, Vol. 19, No. 1, 2016, pp. 88-106.

Olugbenga T.T. and Augie A.I. Estimation of crustal thickness within the Sokoto basin north-western Nigeria using Bouguer gravity anomaly data. WASET, International Journal of Geological and Environmental Engineering, Vol. 14, No. 9, 2020, 247–252.

Osazuwa I.B. and Chii E.C. Two-dimensional electrical resistivity survey around the periphery of an artificial lake in

Bonde D.S., Lawali S., Salako K.A. Structural mapping of solid mineral potential zones over southern part of Kebbi state, northwestern Nigeria. Journal of Scientific and Engineering Research, Vol. 6, No. 7, 2019, pp. 229-240.

Dahlin T., Zhou B. A numerical comparison of 2D resistivity imaging with 10 electrode arrays. Geophysical Prospecting, Vol. 52, 2004, pp. 379-398.

Danbatta U.A. Precambrian crustal development in the northwestern part of Zuru schist belt, northwestern Nigeria. Journal of Mining and Geology, Vol. 44, No. 1, 2008, pp. 43-56.

Danbatta U.A. Precambrian crustal development of the northwestern part of Zuru schist belt, NW Nigeria. A paper presented at the 41st annual conference of Nigerian mining, and geosciences society (NMGS), 2005, Abstr., p. 13.

Danjumma S.G., Bonde D.S., Mohammed A., Lawali S., Birnin Tudu A.M. Identification of mineral deposits in Garin Awwal mining site, Kebbi state, north-western Nigeria. Journal of Multidisciplinary Engineering Science and Technology (JMEST), Vol. 6, No. 6, 2019, pp. 10276-10280.

Ejepu J.S., Unuevho C.I., Agbor A.T., Abdullahi S. Integrated geosciences prospecting for gold mineralization in Kwakuti north-central Nigeria. Journal of Geology and Mining, Vol. 10, No. 7, 2018, pp. 81-94, https://doi.org/10.5897/JGMR 2018.0296.

Fedi M. and Abbas M.A. A fast interpretation of self-potential data using the depth from extreme points method. Geophysics, Vol. 78, No. 2, 2012, pp. 107-116.

Jamaluddeen S.S., Bunawa A.A., Saleh M. An assessment of the groundwater potential of Bayero University Kano Permanent Site using induced polarization and self-potential methods. Journal of Earth science and Engineering, Vol. 4, 2014, pp. 587-596.

Lawal M.M., Salako K.A., Abbas M., Adewumi T., Augie A.I., Khita M. Geophysical investigation of possible gold mineralization potential zones using a combined airborne magnetic data of lower Sokoto basin and its environs northwestern Nigeria. International Journal of Progressive Sciences and Technologies (IJPSAT), Vol. 30, No. 1, 2021, pp. 01-16.

Lawali S., Salako K.A., Bonde D.S. Delineation of mineral potential zones over lower part of Sokoto basin, northwestern Nigeria using aeromagnetic data. Academic Research International, Vol. 11, No. 2, 2020, pp. 19-29.

Lobo-Guerrero A. Application of spontaneous potential profiles for exploration of gold-rich epithermal low sulphidation veins in a humid region. Geoscience Africa 2004, Conference organized by the Geological Society of South Africa in Johannesburg, University of the Witwatersrand, Johannesburg, 2004.

Loke H.M. and Barker R.D. Rapid least-square inversion of apparent resistivity pseudosections. Geophysical Prospecting, Vol. 44(1), 1996, pp. 131-152**,** DOI:10.1111/j.1365-2478. 1996.tb00142.x.

Loke H.M. Tutorial: 2-D and 3-D electrical imaging surveys. Revised edition; 26th July 2004, 128 p.

Oduduru P.I. and Mamah L.I. Integration of electrical resistivity and induced polarization for subsurface imaging around Ihe pond, Nsukka, Anambra basin, Nigeria. Pacific Journal of Science and Technology, Vol. 15, No. 1, 2014, pp. 306-317.

Olalekan O., Afees O., Ayodele S. An Empirical analysis of the contribution of mining sector to economic development in Nigeria. Khazar Journal of Humanities and Social Sciences, Vol. 19, No. 1, 2016, pp. 88-106.

Olugbenga T.T. and Augie A.I. Estimation of crustal thickness within the Sokoto basin north-western Nigeria using Bouguer gravity anomaly data. WASET, International Journal of Geological and Environmental Engineering, Vol. 14, No. 9, 2020, 247–252.

Osazuwa I.B. and Chii E.C. Two-dimensional electrical resistivity survey around the periphery of an artificial lake in

the Precambrian basement complex of northern Nigeria. International Journal of Physical Science, Vol. 5, No. 3, 2010, pp. 238-245.

Ramadan T.M. and Abdel-Fattah M.F. Characterization of gold mineralization in Garin Hawal area, Kebbi state, NW Nigeria using remote sensing. Egyptian Journal of Remote Sensing and Space Science, Vol. 13, No. 2, 2010, pp. 153-163, https://doi.org/10.1016/j.ejrs.2009.08.001.

Sani A.A., Augie A.I., Aku M.O. Analysis of gold mineral potentials in Anka schist belt north western Nigeria using aeromagnetic data interpretation. Journal of the Nigerian Association of Mathematical Physics, Vol. 52, 2019, pp. 291-298.

SARDA – Sokoto agricultural and rural development authority: Sokoto Fadama. Ministry of Solid Minerals Kebbi State, book, 1988.

Shao P., Shang Y., Hasan M., Yi X., Meng H. Integration of ERT, IP and SP methods in hard rock engineering. Applied Sciences, Vol. 11, 2021, 10752. https://doi.org/10.3390/app1122 10752.

Srigutomo W., Trimadona P., Pratomo M. 2D resistivity and induced polarization measurement for manganese ore exploration. Journal of Physics: Conference Series 739, 2016, 012138, https://doi.org/10.1088/1742-6596/739/1/012138.

Telford W.M., Geldart L.P., Sheriff R.E. Applied Geophysics second edition. Cambridge university press. Cambridge, 1990, 744 p.

Unuevho C.I., Amadi A.N., Saidu S., Udensi E.E., Onuoha K.M., Ogunbajo M.I. Geo-electrical prospecting for ore minerals in Kundu western part of Zungeru sheet 163 NW Nigeria. Nigerian Mining Journal, Vol. 14, No. 2, 2016, pp. 73-82.

the Precambrian basement complex of northern Nigeria. International Journal of Physical Science, Vol. 5, No. 3, 2010, pp. 238-245.

Ramadan T.M. and Abdel-Fattah M.F. Characterization of gold mineralization in Garin Hawal area, Kebbi state, NW Nigeria using remote sensing. Egyptian Journal of Remote Sensing and Space Science, Vol. 13, No. 2, 2010, pp. 153-163, https://doi.org/10.1016/j.ejrs.2009.08.001.

Sani A.A., Augie A.I., Aku M.O. Analysis of gold mineral potentials in Anka schist belt north western Nigeria using aeromagnetic data interpretation. Journal of the Nigerian Association of Mathematical Physics, Vol. 52, 2019, pp. 291-298.

SARDA – Sokoto agricultural and rural development authority: Sokoto Fadama. Ministry of Solid Minerals Kebbi State, book, 1988.

Shao P., Shang Y., Hasan M., Yi X., Meng H. Integration of ERT, IP and SP methods in hard rock engineering. Applied Sciences, Vol. 11, 2021, 10752. https://doi.org/10.3390/app1122 10752.

Srigutomo W., Trimadona P., Pratomo M. 2D resistivity and induced polarization measurement for manganese ore exploration. Journal of Physics: Conference Series 739, 2016, 012138, https://doi.org/10.1088/1742-6596/739/1/012138.

Telford W.M., Geldart L.P., Sheriff R.E. Applied Geophysics second edition. Cambridge university press. Cambridge, 1990, 744 p.

Unuevho C.I., Amadi A.N., Saidu S., Udensi E.E., Onuoha K.M., Ogunbajo M.I. Geo-electrical prospecting for ore minerals in Kundu western part of Zungeru sheet 163 NW Nigeria. Nigerian Mining Journal, Vol. 14, No. 2, 2016, pp. 73-82.

КОМПЛЕКСНАЯ 2D ГЕОЭЛЕКТРИЧЕСКАЯ РАЗВЕДКА ДЛЯ ПОИСКА ПОТЕНЦИАЛЬНО ЗОЛОТОНОСНОЙ МИНЕРАЛИЗАЦИИ В ЮЖНОЙ ЧАСТИ КЕББИ, СЕВЕРО-ЗАПАД НИГЕРИИ

Оги А.[1,2], Салако К.А.[2], Рафиу А.А.[2], Химо М.О.[3]

[1]*Факультет прикладной геофизики, Федеральный университет Бирнин Кебби, Нигерия: ai.augie@fubk.edu.ng*

[2]*Факультет геофизики, Федеральный технологический университет Минны, Нигерия*

[3]*Факультет геологии, Федеральный технологический университет Минны, Нигерия*

Резюме. В статье дается детальное геофизическое исследование аномальных зон, выявленных предыдущими аэромагнитными исследованиями в южной части Кебби, северо-запад Нигерии. Комплексные 2D геоэлектроразведочные методы, включающие томографию электрического удельного сопротивления, индукционную поляризацию и собственный электрический потенциал, были использованы для оконтуривания подповерхностной структуры, пригодной для потенциально золотоносной минерализации в частях районов Yauri, Shanga и Magama в штатах Kebbi и Niger на северо-западе Нигерии.

Эти измерения проводились с помощью диполь-дипольной конфигурации и измерителя удельного сопротивления SuperSting. Результаты исследований выявили регионы с низким/высоким удельным сопротивлением, высокой поляризуемостью и высокими значениями собственного электрического потенциала, которые были определены как зоны минерального потенциала. Томография электрического удельного сопротивления помогла очертить области с аномально-низким удельным сопротивлением, которые соответствуют окисленным породам, связанным с прожилками гранита/кварцита. Высокий диапазон удельного сопротивления может существовать на дайковых структурах, связанных с частично разложившимся гранитом и кварцитом, о чем свидетельствуют геологические условия и каротажная диаграмма участка. Метод наведенной поляризации выявил высокую поляризуемость (≥ 20 миллисекунд) в исследуемом районе, возможно, из-за накопления во вмещающих породах рудных минералов, таких как золото. Этот метод также помог выявить регионы с высокими аномалиями индукционной поляризации (≥20 мВ), которые характеризуются жильными минералами руд. Интеграция результатов всех этих методов выявила зоны окисленных пород, дайковые подповерхностные структуры из распавшихся кварцитов, гранитов, гнейсов и жилы рудных минералов. Эти зоны расположены на северо-западе Мараррабы, юго-западе Джинсани и юге Сабон Гари в штатах Нигер и Кебби и их можно рассматривать как потенциал для разведки и добычи золота.

Ключевые слова: *2D-моделирование, томография электрического удельного сопротивления, индукционная поляризация, собственный электрический потенциал, золотое оруденение*

ŞİMALI-QƏRBİ NİGERİYA, KEBBİNİN CƏNUB HİSSƏSİNDƏ POTENSİAL QIZILDAŞIYAN MİNERALİZASİYANIN AXTARIŞI ÜÇÜN KOMPLEKS 2D GEOELEKTRİK KƏŞFİYYATI

Augie A.I.[1,2], Salako K.A.[2], Rafiu A.A.[2], Jimoh M.O.[3]
[1]Tətbiqi geofizika fakültəsi, Birnin Kebbi federal universiteti,Nigeriya: ai.augie@fubk.edu.ng
[2]Geofizika fakültəsi, Minnı Federal texnoloji universiteti, Nigeriya
[3]Geologiya fakültəsi, Minnı Federal texnoloji universiteti, Nigeriya

Xülasə. Əvvəllər bu rayonda aeromagnit tədqiqatlarla aşkar edilmiş anomal zonaların dəqiq geofiziki tədqiqatları aparılmışdır. Tomoqrafik elektrik xüsusi müqavimət, induksiya polyarizasiyası və məxsusi elektrik potensialı ehtiva edən, kompleks 2D geo-elektrokəşfiyyat metodları Şimali-Qərbi Nigeriyanın Kebbi və Niger ştatlarının Yauri, Shanga həmçinin Magama rayonlarında potensial qızıldaşıyan mineralizasiyanın səthaltı strukturun konturlaşdırılması üçün istifadə edilmişdir.

Bu ölçülmələr dipol-dipol konfigurasiyası və SuperSting xüsusi müqavimətin ölçülməsi üsulu ilə aparılmışdır. Tədqiqatların nəticələri əsasında aşağı/yüksək xüsusi müqavimət, yüksək polyarlaşma, məxsusi elektrik potensiallı regionlar aşkar edilmişdir ki, onlar mineral potensiallı obyektlər kimi təyin edilmişdir. Xüsusi müqavimətin elektrik tomoqrafiyası, qranat/kvarsit damarcıqları ilə əlaqədar oksidləşmiş süxürlara müvafiq anomal aşağı xüsusi müqavimətə malik, sahələri cizgiləməyə imkan verdi.

Xüsusi müqavimətin yüksək diapazonu qismən dağılmış qranit və kvarsla əlaqədar dayka strukturlarında mövcud ola bilər ki, bunu geoloji şəraitlər və sahənin karotaj diaqramı əks etdirir. Yönəldilmiş polyarizasiya metodu tədqiq olunan rayonda yüksək polyarlaşma (≥ 20 millisaniyə) fiksasiya etmişdir. Bu çox güman ki, filiz minerallarının (qızıl) yerləşdirici süxürlarında toplanması ilə əlaqədardır. Bu metod həmçinin filizlərin damar mineralları ilə səciyyələnən yüksək anomal induksiyon polyarizasiyasına malik (≥20 мВ) regionları aşkar etməyə imkan yaratmışdır. Bütün bu metodların nəticələrinin inteqrasiyası oksidləşmiş süxurların zonalarını, dağılmış kvarsitlərin, qranitlərin, qneyslərin və filiz minerallarının nüvələrinin dayk yeraltı quruluşlarını aşkar etmişdir.

Bu zonalar şimal-qərbi Mararabı, cənub-qərbi Cinsani və Sabon Garinin cənubunda, Niger, Kabbi ştatlarında yerləşir. Onlar qızıl kəşfiyyatı və hasilatı üçün potensial kimi qəbul edilə bilər.

Açar sözlər: *2D-modelləşdirmə, elektrik xüsusi müqavimət tomoqrafiyası, induksiya polyarlaşması, məxsusi elektrik potensialı, qızıl filizləşməsi*